A One-Dimensional Numerical Vertical Mixing Model with Application to Western Lake Erie

Lyon W. J. Lanerolle, Richard P. Stumpf,
Timothy T. Wynne and Richard C. Patchen

2011

A NOAA Technical Memorandum
NOS NCCOS 131

Mention of trade names or commercial products does not constitute endorsement or recommendation for their use by the United States government.

Citation for the Full Report:
Lanerolle, L.W.J., R.P. Stumpf, T.T. Wynne and R.C. Patchen. 2011. A One-Dimensional Numerical Vertical Mixing Model with Application to Western Lake Erie. NOAA Technical Memorandum NOS NCCOS 131. National Oceanic and Atmospheric Administration, National Ocean Service, National Centers for Coastal Ocean Science. Silver Spring, MD. 44 pp.

A One-Dimensional Numerical Vertical Mixing Model with Application to Western Lake Erie

Lyon W. J. Lanerolle[1,2], Richard P. Stumpf[3], Timothy T. Wynne[3] and Richard C. Patchen[1]

[1]NOAA/National Ocean Service/Coast Survey Development Laboratory, 1315 East-West Highway, Silver Spring, MD 20910; [2]Earth Resources Technology (ERT) Inc., 10810 Guilford Road, Suite 105, Annapolis Junction, MD 20701; [3]NOAA/National Ocean Service/National Centers for Coastal Ocean Science, 1305 East-West Highway, Silver Spring, MD 20910.

Table of Contents

List of Figures

Executive Summary

Cyanobacterial (for example, Microcystis) blooms give rise to scum which occurs in western Lake Erie. The bacterial cells do not have a swimming capability but can regulate their buoyancy by varying their carbohydrate content. Due to buoyancy, their distribution within the water column is influenced by the vertical eddy-viscosity which easily overcomes the variable buoyancy forces. This eddy-viscosity is generated primarily by meteorological forcing over the shallow lake bathymetry. In order to understand how this is accomplished, its nature and to study its dispersive effects, a one-dimensional numerical ocean modeling set-up based on Rutgers University's Regional Ocean Modeling System (ROMS) was constructed and tested.

This set-up was also designed to have a high degree of portability in that it could be easily applied to any open water body using the following as inputs: a set of temperature and salinity initialization profiles, a representative bathymetric depth value, a representative Coriolis parameter and a fixed point time-series of meteorological variables to aid in the imposition of surface wind stresses and the net heat flux.

In order to isolate the most reasonable choices for model open boundary conditions, vertical eddy-viscosity scheme(s) and Jerlov light attenuation parameter (as the western Lake Erie region is sometimes known to be murky), a series of model calibration exercises were conducted using the west Florida shelf region as an example. They indicated that the best choices for open boundary conditions were the wall/closed conditions, the vertical eddy-viscosity scheme(s) were the Mellor-Yamada 2.5 and GLS k-ω schemes, and for light attenuation, a Jerlov number of one.

Using this model configuration, the vertical mixing modeling set-up was applied to western Lake Erie employing a bathymetric depth value and a Coriolis parameter representative of this geographical region. The initial conditions for temperature were derived from observations and the salinity was zero as the lake is purely fresh. The meteorological forcing variables were a combination of observations from the NDBC Marblehead, OH station and some North American Regional Reanalysis (NARR) products (for the radiation fluxes). As in the calibration runs, here too the modeling set-up was always numerically stable and stability was monitored via the Courant-Lewy-Friedrichs (CFL) parameter. The model set-up was validated by comparing the predicted surface and bottom temperatures with observations which agreed to within 1 ^{o}C and 0.5 ^{o}C respectively. An examination of the Péclet/Reynolds number showed that the modeled vertical dynamics of western Lake Erie are driven by viscous/diffusive processes as opposed to inertial/advective processes.

Finally, using the main output from this modeling set-up – the vertical eddy-viscosity, a series of passive tracer and Lagrangian particle path tracking experiments were conducted in order to examine how scum forming cyanobacteria would respond to vertical mixing. They correctly predicted the large and rapid mixing associated with the high viscosity values and the stagnation/accumulation associated with the low values. These tracer and particle tracking tools are sufficiently general in that they can be employed with any time-evolving, one-dimensional field of vertical eddy-viscosity to study tracer/particle dispersal situations.

1.0 Introduction and Motivation

Cyanobacterial blooms are seasonal and occur yearly in the western section of Lake Erie, MI. When positively buoyant, blooms result in scum layers which float at the lake surface and are capable of harming humans and animals due to being a hepatotoxin, interference with fishing activities and of the degradation of the scenic nature of that area.

Such scum forming cyanobacterial cells, although variably buoyant, do not have a swimming capability and are transported up and down the water column due to the action of vertical eddy-viscosity. The eddy-viscosity in turn is generated by a combination of factors : shallowness of this region of the lake, the action of winds and possibly also the vertical temperature stratification. As the lake is purely fresh, its salinity is zero.

In an attempt to understand how the meteorological conditions in the western Lake Erie region give rise to eddy-viscosity fields which allow cyanobacterial movement within the water column, a one-dimensional numerical ocean model application was established. The ocean model selected for this purpose was Rutgers University's Regional Ocean Modeling System (ROMS). ROMS is a split-explicit, finite difference based orthogonal, curvilinear grid numerical ocean model (Shchepetkin and McWilliams, 2004). The vertical grid is of a stretched, terrain-following, sigma coordinate (Song and Haidvogel, 1994) type. The momentum and tracer advection terms are discretized using high resolution, third order upstream-biased advection schemes which alleviate the need to add explicit horizontal viscosity/diffusivity in the numerical computations (Shchepetkin and McWilliams, 1998). The hydrostatic pressure gradient terms are also discretized using an extremely robust and accurate piecewise cubic spline construction (Shchepetkin and McWilliams, 2003). The vertical turbulence/eddy mixing is carried out using a standard Mellor-Yamada 2.5 scheme (Mellor and Yamada, 1982), a non-local K-Profile Parameterization (KPP) scheme or a family of General Length Scale (GLS) schemes consisting of k-ε, k-τ and k-ω schemes (Warner et. al., 2005). Along the ocean bottom bathymetry, friction can be prescribed with a logarithmic, linear, quadratic law or a Bottom Boundary Layer (BBL) formulation (Styles and Glenn, 2000). At the ocean surface, the surface meteorological forcing can be imposed in two ways in ROMS – *(a)* if the wind stresses and net heat fluxes are available then, they can be prescribed directly but otherwise, *(b)* the wind speeds, air pressure, air temperature, relative humidity, net shortwave radiation flux and downward longwave radiation flux observations when available are specified and then the wind stresses and the net heat flux are estimated internally using a Bulk Flux formulation (Liu et. al, 1979; Fairall et. al, 1996a,b). If downward longwave radiation data is unavailable, the net longwave radiation can be computed internally using the Berliand formulation (Berliand and Berliand, 1952). ROMS also has the ability to account for light attenuation properties of the water using a Jerlov number-based formulation which applies exponential decay functions to the

net shortwave radiation fluxes (Paulson et. al., 1977). The perfect restart mechanism contained in the ROMS allows lengthy computations to be carried out in reasonably sized run segments.

A primary requirement of this modeling set-up was portability whereby it could be easily applied to any water body using a minimum of model inputs and it was designed with this requirement in mind. Provided that the spatial extent of the horizontal grid is not too small, it can be easily applied anywhere with the following inputs : a set of T, S initialization vertical profiles, a representative bathymetric depth value, a representative Coriolis parameter and a fixed point time-series of meteorological variables.

After setting up an idealized, one-dimensional ROMS configuration, a series of test runs were performed to decide on the best choices for the (i) open ocean boundary condition set, (ii) vertical eddy-viscosity scheme(s), and (iii) Jerlov number (that is, the water type). Thereafter, using these ideal choices, the ROMS set-up was applied to the western Lake Erie geographical region. The model predicted temperature fields were validated against observations and the agreement was found to be very good thereby attesting to the validity of the modeling set-up. Furthermore, an examination of the Péclet/Reynolds number showed that the modeled vertical dynamics of western Lake Erie are driven by viscous/diffusive processes as opposed to inertial/advective processes.

The primary output product of interest of this modeling set-up is the vertical eddy-viscosity which describes the strength and nature of the vertical mixing. Using the spatio-temporal eddy-viscosity field generated by the western Lake Erie application, a series of passive tracer and Lagrangian particle path evolution exercises were carried out which showed that their response to the viscosity accurately characterized the associated vertical mixing.

This article is organized as follows: the next section (Section 2) describes how the ROMS model grid and the model itself was set-up for a one-dimensional, vertical mixing configuration and thereafter, Section 3 outlines the model calibration exercises undertaken in order to discover the ideal set-up parameters (that is, the best open ocean boundary conditions, vertical-eddy viscosity scheme(s) and Jerolov water type choices). Section 4 explains how this ROMS set-up was applied to the western Lake Erie region and the ensuing results and their discussion. The passive tracer and Lagrangian particle path vertical mixing experiments using the eddy-viscosity are described in Section 5. Finally, a summary and some conclusions pertaining to this research are provided in Section 6.

2.0 **Numerical Model Set-up**

Even though this modeling set-up was meant to be one-dimensional, due to ROMS being a three-dimensional model, it needed to be set-up in a (quasi) three-dimensional configuration. The one-dimensionality was invoked via (1) the four model open boundary conditions (ROMS requires any

domain to have four corners/boundaries) chosen to be of the same mathematical type without any discrimination or bias towards a particular boundary, (2) the use of a constant bathymetry in the horizontal, (3) the horizontal spatial extent of the domain being physically small (for example 50 km x 50 km), (4) the use of a constant Coriolis parameter in the horizontal, (5) the placement of the majority of the grid points in the vertical direction with a few grid points in each of the horizontal directions, (6) the use of initialization temperature (T) and salinity (S) fields which are invariant in the horizontal directions and which only vary in the vertical are thus simply vertical profiles, and (7) fixed point time-series of meteorological variables which too are constant in the horizontal.

Along the four boundaries, ROMS permits the use of (a) radiation conditions or (b) wall/closed conditions or (c) periodic conditions. Section 3.0 describes the numerical experiments carried out with each of these boundary conditions and their outcomes. The bathymetry is specified by looking at the geographical region of application and then selecting a representative bathymetric value (for example, an average value) for it. It is not expected to vary much in space due to the limited spatial extent of the computational domain. Similarly, the Coriolis parameter is selected by taking in to account a representative latitude for the domain. The model is spun-up from rest (that is, zero velocities and water level/elevation) and the ensuing flow develops in response to (i) the temperature (T) and salinity (S) initialization fields and (ii) the meteorological forcing applied at the surface. The T and S initialization profiles can be obtained from climatological fields or from observations. The meteorological forcing is generated through the ROMS Bulk Flux formulation which requires winds, air temperature, air pressure, air relative humidity, net shortwave radiation and downward longwave radiation as inputs to calculate the surface wind stresses and the net heat flux. Fixed point time-series for these variables can be obtained from observations or from model generated products such as those from the North American Regional Re-analysis (NARR) (NARR, 2009) products. Tidal dynamics were not included in the model set-up.

With regards to the ROMS model algorithmic configuration options, the following were selected: (i) the UNESCO non-linear equation of state to estimate water density (Jackett and McDougall, 1995), (ii) upstream-biased horizontal advection of momentum and tracers which alleviates the need to use explicit horizontal numerical viscosity/diffusivity, (iii) spline vertical advection, (iv) quadratic bottom drag formulation, (v) either the Mellor-Yamada 2.5 or the GLS family of vertical eddy-viscosity schemes, (vi) variable Jerlov number light attenuation formulation, and (vii) the Bulk Flux formulation described in Section 1.0 (Introduction) in order to calculate the ocean surface wind stresses and net heat fluxes.

3.0 **Model Calibration**

In order to isolate the most reasonable choices for model open boundary conditions, vertical eddy-viscosity scheme(s) and the Jerlov water type, a set of numerical model calibration experiments were

performed. An orthogonal, curvilinear grid containing 9 x 9 points in the horizontal covering a area of ~20 km x 20 km was generated using the Matlab-based SeaGrid tool (SeaGrid, 2009) and it was situated on the west Florida shelf. In the vertical, a terrain following σ-grid formulation was employed with 20 model vertical levels; several parameter sets were tested including those which produced a uniform vertical grid (with zero stretching) and the numerical predictions were found to be quite similar which could be due to shallowness and lack of spatial variation in the bathymetry. The modeling set-up used for these experiments involved the use of (i) idealized initial vertical T and S profiles as initial conditions, (ii) a constant bathymetry of 10m, (iii) a Coriolis parameter corresponding to a location on the west Florida shelf (between Tampa Bay and Charlotte Harbor in Florida) and (iii) meteorological variables (winds, air temperature, air pressure, relative humidity, net shortwave radiation flux, downward longwave radiation flux) from NARR for a time period in 2004. The NARR time-series were taken from its grid point closest to the centroid of the the model grid. This geographic region was selected because of the availability of data and previous studies conducted there (Lanerolle, et. al, [2006]; Lanerolle et. al, [2009a]; Lanerolle et. al, [2009b]). The model grid is shown in Figure 1, the initial T and S profiles are plotted in Figure 2 and the NARR surface forcing meteorological variables are plotted as time-series in Figure 3. The winds provided by NARR were prescribed at a height of 10m above the ocean surface and the air temperature and relative humidity were values from a height of 2m. The meteorological conditions show a mild wind period (~5 m/s) with a gentle heating trend in terms of the air temperature; the other variables conform to average/expected conditions. The shortwave radiation plot shows relatively cloud-free conditions.

In the model simulations, the background viscosity and diffusivity coefficients were set to a value of 1 x 10^{-8} m^2/s and it is known that the vertical T and S stratification are sensitive to their level (Lanerolle et. al, [2009b]). The quadratic bottom drag coefficient employed was 0.003 in value. The baroclinic time step employed was 300s and the corresponding barotropic time step was 15s. Stations archives of the model output variables were stored in time at an hourlyfrequency and the archive location was the grid point corresponding to the centroid of the model grid (Figure 1). As this ROMS application employed relatively few grid points and a relatively large baroclinic time step, it was possible to carry out the simulations in serial mode without the need for MPI parallelization. A 30-day simulation consumed approximately 1 minute of wall clock time on a dual core Dell PowerEdge SC 1470 platform (using Red Hat Enterprise Linux) attesting to the efficiency and expediency of this modeling set-up.

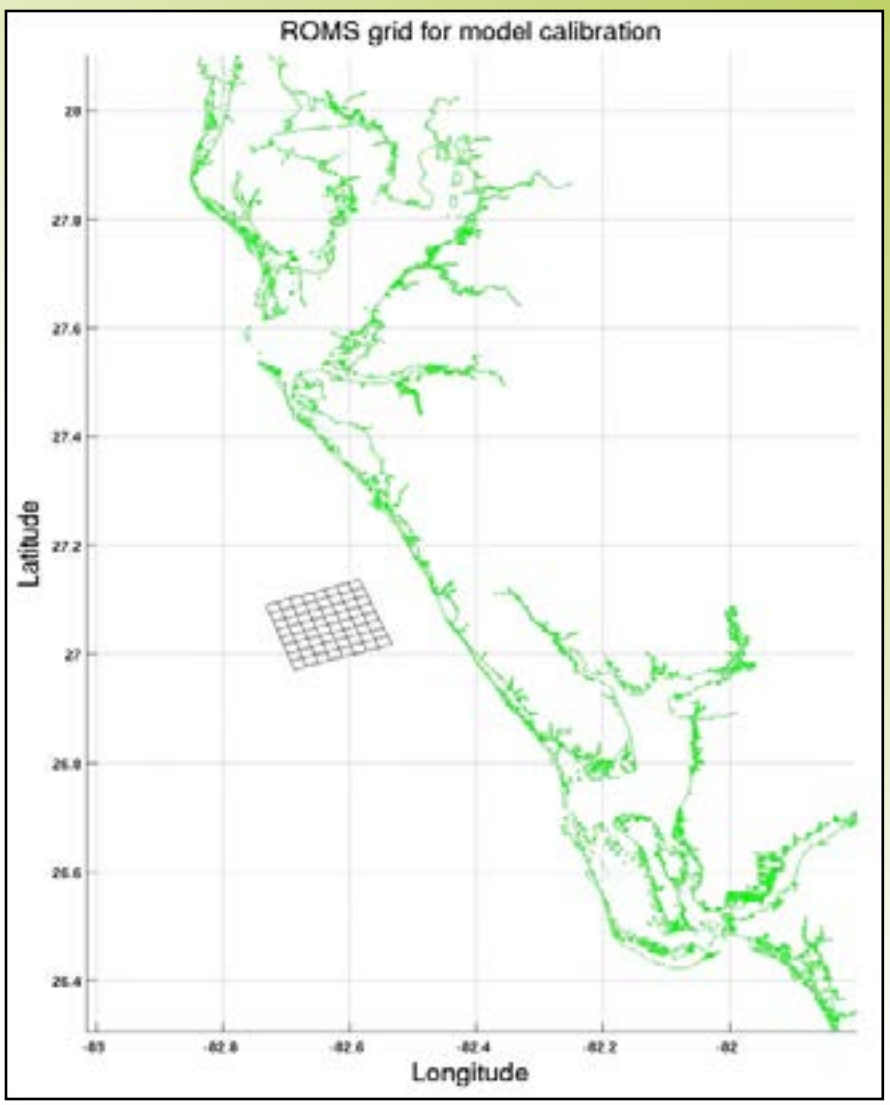

Figure 1: ROMS grid on the west Florida shelf employed for model calibration.

3.1 **Sensitivity to Choice of Open Boundary Conditions**

Four different open boundary condition options available within ROMS were examined. They are : radiation conditions, closed conditions, wall conditions and doubly periodic (in both the meridional and zonal directions) conditions. As this set-up is meant to be a one-dimensional, generic, portable and open ocean/water body configuration, the same boundary conditions were applied on all four open boundaries without any discrimination. In all cases, it is the Mellor-Yamada 2.5 vertical eddy-viscosity closure that was used. The total simulation duration was 90 days. The results are given in Appendix A and to highlight the spatio-temporal evolution of the numerical predictions more clearly, only the first 30 days of simulations are shown.

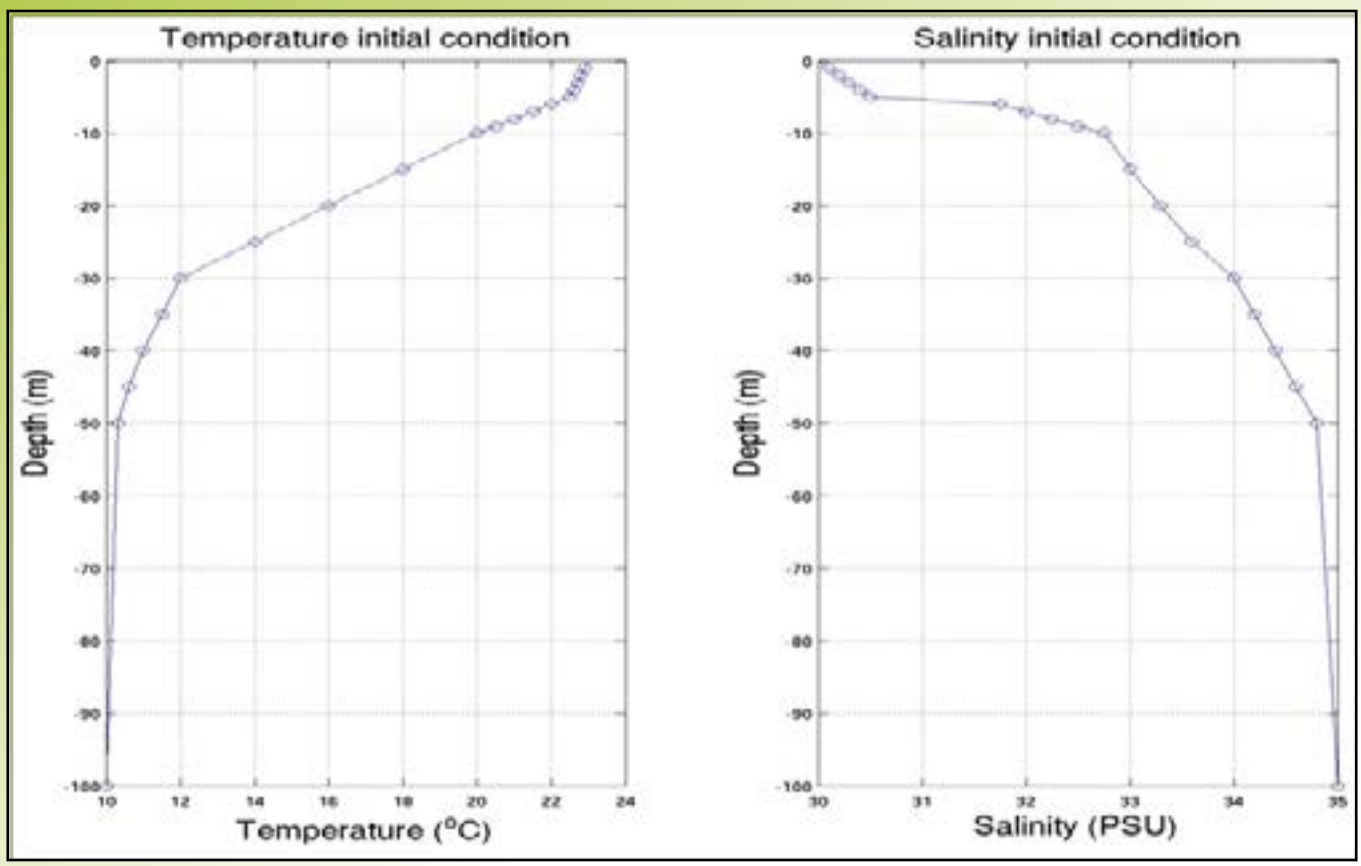

Figure 2 : T and S vertical profiles used for model initialization in the calibration experiments.

The Courant-Lewy-Friedrichs (CFL) number is a measure of numerical stability of this modeling set up because : (i) no explicit numerical horizontal or vertical viscosity/diffusivity is employed in this ROMS application (as a result of utilizing the upstream-biased oscillation- free discretization options for the advection of momentum and tracers) and (ii) the vertical viscosity/diffusivity is treated in an implicit manner.

Figure A1 shows that the CFL number is well below unity and hence the computation are numerically stable (and, this is also true for the full 90-days of the simulation); the kinetic, potential and total energy time-series plots show that the radiation conditions allow the model free-surface/water elevations to evolve in an uncontrolled manner thus leading to large fluctuations in potential energy and the periodic boundary conditions allow large variations in the meriodional and zonal currents leading to large fluctuations in the kinetic energy. Figure A2 shows the spatio-temporal evolution of the vertical w-velocity/current and the radiation conditions produce a visible deformation of the ocean free-surface and the periodic boundary conditions dampen the vertical velocities (due to the elimination of the horizontal gradients in the currents). The evolution of temperature is shown in Figure A3 and yet again, after ~20 days of computation, the periodic boundary conditions destroy the vertical stratification (as also in the w-velocities) and the radiation conditions generate less heating than the closed or wall conditions;

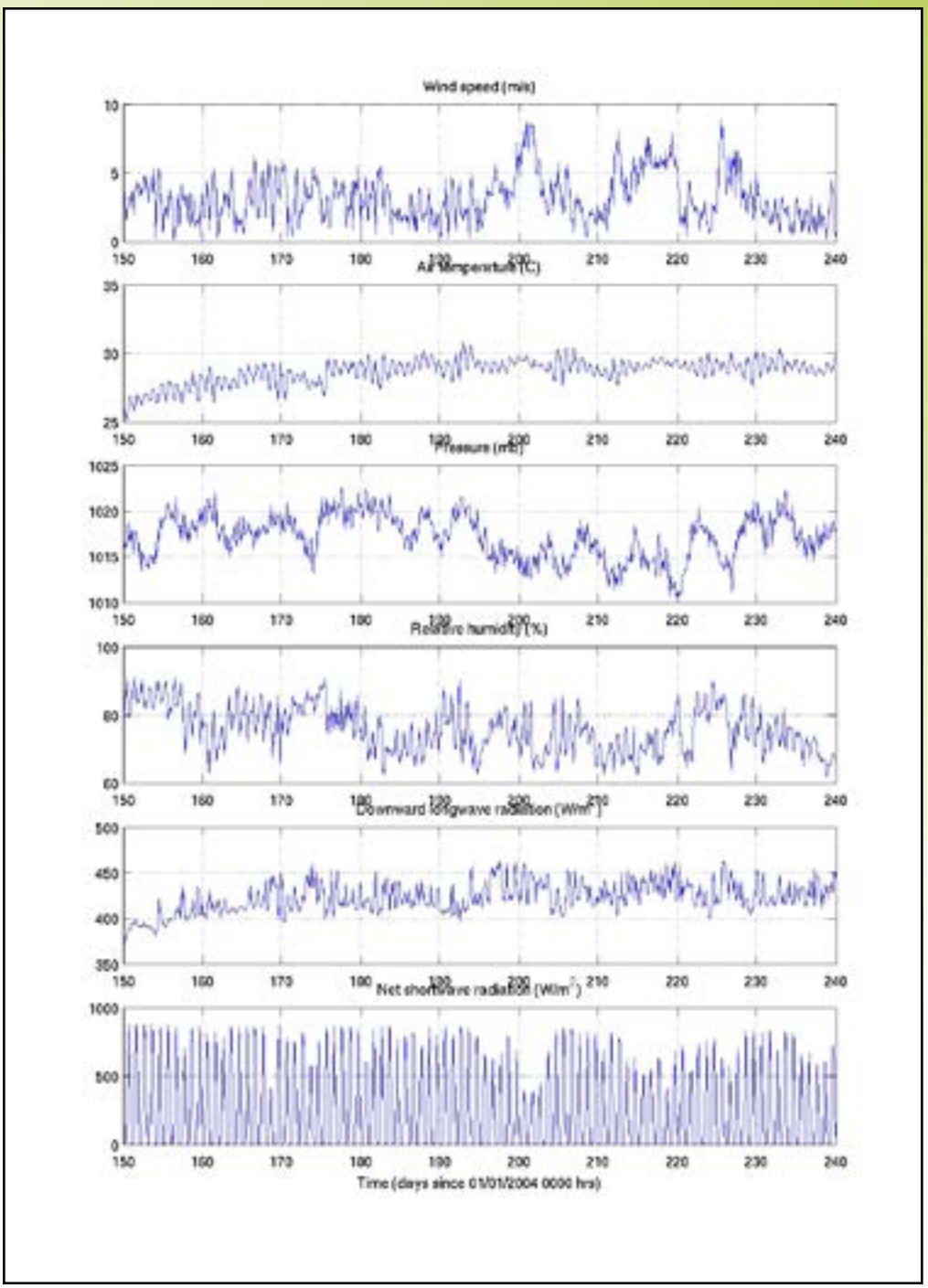

Figure 3 : Time-series of meteorological variables used for the surface forcing in the calibration experiments.

this is expected because the radiation conditions allow heat to flow out of the computational domain whereas the wall/closed conditions do not and are effectively insulating conditions. The diurnal heating patterns due to the shortwave radiation flux are also visible. It was decided to focus the tracer evolution on the temperature because eventually this modeling set-up will be applied to western Lake Erie where the water is purely fresh (zero salinity). The density anomaly plot in Figure A4 shows a similar trend to those of temperature but also that the water columns are geostrophically stratified and

stable with the heaviest water near the bottom and the lightest near the surface, as expected. Finally, Figure A5 shows the vertical eddy-viscosity evolution (its logarithm, to a base of ten) and the closed/wall conditions provide stronger mixing near the surface than the radiation conditions; the periodic boundary conditions destroy the bottom boundary layer and enhance the surface mixing and extend it down the water column.

The results given in Appendix A and the above discussion lead to the conclusion that the best compromise in terms of open boundary condition choices are the wall/closed conditions both of which appear to function identically. Therefore, hearafter, these conditions will be adopted in the ROMS vertical mixing modeling set-up.

3.2 **Sensitivity to Choice of Vertical Eddy-Viscosity Closure Scheme**

Using the wall/closed open boundary conditions (Section 3.1), two sets of vertical eddy-viscosity models were tested. The first was the standard Mellor-Yamada 2.5 scheme and the second was the family of GLS schemes; in the latter, the kkl, k-ε and k-ω members were selected. The outcome of the numerical experiments is given in Appendix B and the computations were carried out for the full 90-days.

In Figure B1, the CFL number time-histories show that the GLS models generate higher CFL values than the Mellor-Yamada model but they still are well below unity thus ensuring the numerical stability of the ROMS computations. The time-series of the energetic quantities (kinetic, potential and total energies) show that they are quite similar to each other for the different eddy-viscosity schemes. The vertical w-velocities in Figure B2 show that those for the GLS schemes are quite similar to each other and are also similar to the velocities resulting from the Mellor-Yamada model with the exception that the former are larger in magnitude (both in terms of positive and negative values). The temperature and density anomaly evolution plots in Figures B3 and B4 show that with time, the water column gets completely mixed but the mixing associated with the GLS models is more severe where after ~50 days in to the computation, it is fully mixed. For an impermeable, wall/closed open boundary configuration, such a fully mixed eventuality is the expected scenario. The resulting temperatures and density anomalies due to the three GLS schemes are similar. This increased mixing associated with the GLS schemes is due to them having a higher background viscosity value (1.0×10^{-5} m^2/s) built in to them and which cannot be controlled externally (unlike in the Mellor-Yamada scheme) and this is also evident from the eddy-viscosity plots in Figure B5. As before, density anomaly plots show that the water column is geostrophically stable. Finally, the vertical eddy-viscosity evolution fields (their logarithms, to a base ten) in Figure B5 show that those from the three GLS models are similar to each other and unlike the Mellor-Yamada field, from time to time, they possess high values which extend throughout the full depth of the water column. The higher background viscosity value associated with the

GLS models is evident from these plots and the increased eddy-viscosity values during the relatively strong wind speeds (Figure 3) is also clearly seen.

The above numerical experiments lead to the conclusion that the different GLS models exhibit similar behavior which is different to that of the Mellor-Yamada model. A ROMS application to the Chesapeake Bay, (Lanerolle et. al. [2009c]) has shown that the best overall temperature and salinity stratification was achieved via the GLS k-ω scheme. Therefore, to better understand the implications of choosing a vertical eddy-viscosity scheme for this application, the Mellor-Yamada and the GLS k-ω model are selected for further investigation.

3.3 Sensitivity to Choice of the Jerlov Water Type

It is known that the waters in western Lake Erie can be murky and hence, the capabilities of the ROMS light attenuation algorithm were examined. The algorithm attenuates the incident downward shortwave radiation using a Jerlov parameter based formulation. This parameter ranges in value from 1 to 5 with a value of 5 generating the strongest attenuation. The one-dimensional vertical mixing set-up was tested for extreme Jerlov parameter values during which the set-up employed (i) the wall/closed open boundary conditions and (ii) the Mellor-Yamada and GLS k-ω vertical eddy-viscosity schemes. The results over a 90-day simulation period are provided in Appendix C.

The plots of kinetic, potential and total specific energies in Figure C1 show that with the increase of the Jerlov number is seen as a reduction (although not dramatic) in both the kinetic and potential (and hence total) energies. The CFL number however still remains less than unity throughout the simulations period thus ensuring their numerical stability. The spatio-temporal evolution of the vertical w-velocities in Figure C2 show that increased Jerlov numbers tend to dampen the velocities, an effect which increases with time; this behavior is seen in both the Mellor-Yamada and GLS k-ω model simulations. Figures C3 and C4 show the evolution of the temperature and density anomaly respectively and they indicate that increasing the Jerlov number destroys the vertical stratification sooner in time and that there is not much of a difference in the results between Jerlov numbers 4 and 5. As before, density anomaly plots show that in all cases, the water column remains geostrophically stable in time. Finally, the vertical eddy-viscosity (its logarithm, to a base of ten) evolution plots in Figure C5 clearly show the effects of increasing the Jerlov number whereby a dramatic increase in the eddy-viscosity is seen both in time and also throughout the water column thus significantly increasing the vertical mixing associated with the modeling set-up. It is this increased vertical mixing and the destruction of the vertical stratification which leads to the lower specific kinetic and potential energies as seen in Figure C1.

The results given in Appendix C show that increasing the Jerlov number has significant detrimental effects on the vertical stratification and the vertical eddy-viscosities. It is expected that these effects are more severely pronounced due to the shallowness (10m) of the bathymetry which is typical of the applications this vertical mixing modeling set-up is designed for. Therefore, a Jerlov number of 1 will be adopted for this modeling set-up.

4.0 **Western Lake Erie Simulation, Results and Discussion**

Using the most reasonable configuration choices (wall/closed conditions for the open boundaries, Mellor-Yamada and GLS k-omega vertical eddy-viscosity schemes and a Jerlov light attenuation number of one), a one-dimensional ROMS vertical mixing set-up was implemented for western Lake Erie. As for the calibration exercises, the grid had 9 x 9 points in the horizontal and 20 levels were used in the vertical. The Coriolis parameter employed corresponded to the latitude of the centroid of the model grid, the bottom bathymetry was 7.7 m (from observations) and these two parameters were uniform in the horizontal. The model domain and grid are plotted in Figure 4.

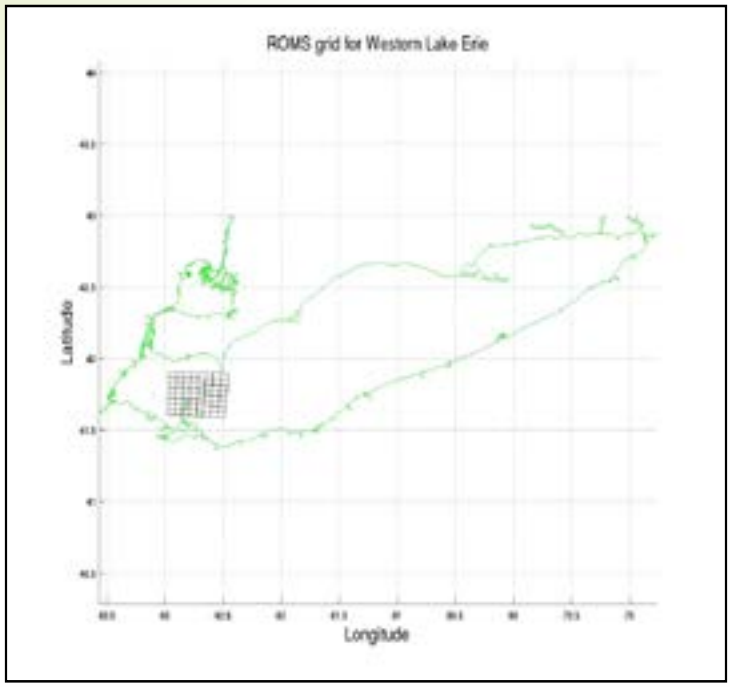

Figure 4 : ROMS grid employed for the western Lake Erie simulation.

The initial conditions for temperature were formed by linearly interpolating in the vertical a surface (25.805 ^{o}C) and a bottom (25.260 ^{o}C) observed value corresponding to August 01, 2008. As Lake Erie is purely fresh, the salinity was taken to be zero.

As in the calibration experiments, the meteorological forcing was specified as a single point time-series without any spatial variation. The winds, air temperature, barometric pressure and relative

humidity variables were obtained from the NOAA/National Data Buoy Center (NDBC) observations at Marblehead, OH (station 9063079). The downward longwave and net shortwave radiation flux time-series were obtained from NARR at the grid point which was closest to the centroid of the model grid. The meteorological variables are plotted in Figure 5 and it is seen that there is an even around day 258. The NARR generated net shortwave radiation flux was reduced by 20% on the assumption that this would make them match better with observations as also seen in a previous study (Lanerolle et. al., [2009b]).

The ROMS simulation was carried from August 01, 2008 to October 31, 2008 (90 days) using the same model configuration as for the calibration experiments and also with a 300 second baroclinic time step. The wall clock run time consumed for these simulations was identical to that of the calibration experiments. The results of the simulation are given in Appendix D.

The CFL number time-histories plotted in Figure D1 indicate that they are well below unity and hence the ROMS simulations are numerically stable. The Mellor-Yamada and the GLS k-ω models yield similar CFL number values and they tend to peak at times where the wind speeds also peak. Figure D2 shows the vertical w-velocities; the two eddy-viscosity models generate very similar fields and for the majority of the time, these velocities are quite small (~1 x 10^{-5} m/s). The temperature and density anomaly fields in Figures D3 and D4 respectively also show strong similarities between the two sets of eddy-viscosity models and weak vertical stratification; most of the stratification is near the ocean surface and appears to be induced by the meteorological forcing applied in the simulations. The lack of stratification is not surprising considering the weak stratification present in the temperature initialization field. Seasonal cooling in the temperature fields is seen and this is consistent with the air temperatures shown in Figure 5 which gives the expected response in the density anomaly fields (Figure D4). For example, for purely fresh water, the density anomalies at 26 ^{o}C and at 12 ^{o}C are -3.2 Kg/m^3 and -0.5 Kg/m^3 respectively (Water density calculator, [2009]). Figure D4 also attests to the fact that the water column is geostrophically stable. The vertical eddy-viscosity plots in Figure D5 show that unlike in the calibration experiments (with low Jerlov numbers), for this realistic application, relatively high values of viscosity are present throughout the water column and for much of the time, thus implying the presence of strong vertical mixing. The high values of eddy-viscosity clearly correspond to the times when the winds speeds are relatively high (Figure 5) with the exception of the period during the meteorological even around day 258. Although the viscosities resulting from the Mellor-Yamada and GLS k-ω schemes are similar, there are also some difference in that : (i) the background level of the former is lower than that of the latter and (ii) although near the ocean surface, both models generate similar viscosity values but near the bottom, the latter has appreciably larger values. Figure D6 shows comparisons of the surface and bottom temperatures from the ROMS predictions against observations; the observations around day 258 are either missing or unreliable, perhaps due to an equipment malfunction resulting from the meteorological event. These plots show that the simulated temperatures

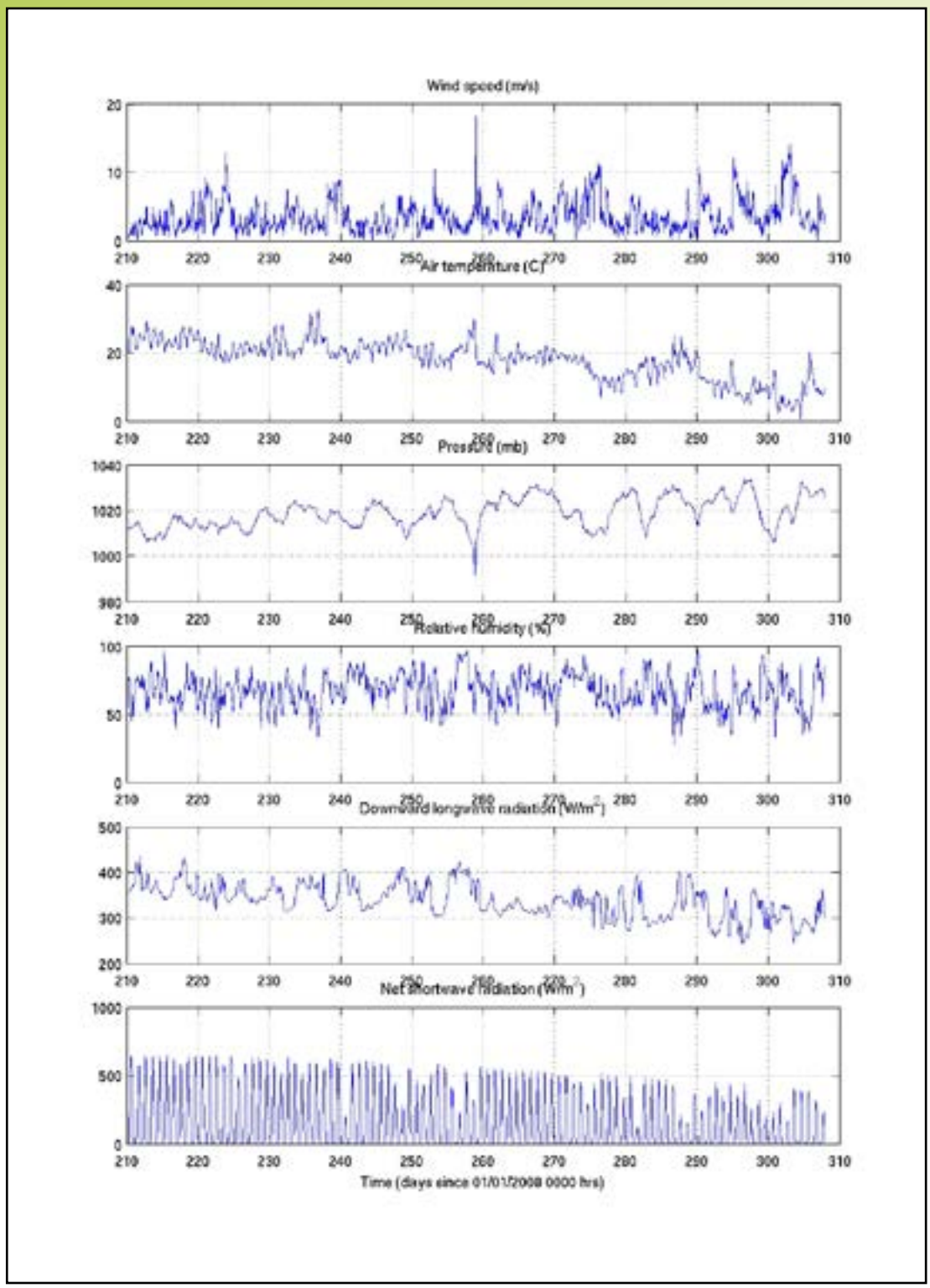

Figure 5: Time-series of meteorological variables used for the surface forcing in the western Lake Erie synoptic hindcast simulation.

follow the observations closely and are able to follow the trends (for example, the peaks) well. At the surface, the predicted temperatures are within 1^{o} C of the observations and at the bottom they are within 0.5^{o} C. The model is always warmer relative to the observations and the 20% reduction factor in the net shortwave radiation flux perhaps needs some refinement in value. The numerical predictions

resulting from the two eddy-viscosity models are seen to be in very close agreement with each other. This comparison therefore serves to prove the validity of this simple one-dimensional vertical mixing modeling set-up.

The Péclet number for mass diffusion is a measure of the relative strength of advective processes over diffusive processes and it is defined as Pe=U·L/D where U is a characteristic advective speed, L is a characteristic length scale and D is a characteristic viscosity/diffusivity coefficient. This is also the Reynods number, Re, which is a measure of the ratio of inertial forces to viscous forces. This parameter is dimensionless. Generally, if Pe » 1, advective processes dominate and if Pe « 1 then, the diffusive processes dominate. For the western Lake Erie mixing model, in the vertical direction, in terms of Order of Magnitude (OM) values, L ~ 1 m (as the bathymetry is 7.7 m), U ~ 1.0 x 10^{-5} m/s (a mean vertical w-velocity from Figure D2) and D ~ 1.0 x 10^{-3} m^2/s (a mean vertical eddy-viscosity from Figure D5) so that Pe=1.0 x 1.0 x 10^{-5} / 1.0 x 10^{-3} = 0.01 « 1. Hence, the simulated western Lake Erie results indicate that it is dominated by viscous/diffusive processes in the vertical.

5.0 **Idealized Vertical Mixing Numerical Experiments**

It was attempted to investigate in a very simplistic manner (zeroth order method and without engaging in an exhaustive survey of the scientific literature) as to how a passive tracer and an ensemble of mass-less and point-like Lagrangian particles would respond to the vertical eddy-viscosity fields associated with the western Lake Erie ROMS simulations. Such an exercise is expected to reveal how scum forming cyanobacteria in the water column would respond to vertical mixing.

5.1 **Passive Tracer Approach**

As the physics of western Lake Erie in the vertical was shown to be dominated by viscous/diffusive processes, a passive tracer would obey the following equation in the vertical (*z*) direction

$$\frac{\partial C}{\partial t} - \frac{\partial}{\partial z}\left(K\frac{\partial C}{\partial z}\right) = 0$$

where $C = C(z,t)$ is the tracer concentration and $K = K(z,t)$ is the eddy-viscosity which is known from the ROMS simulations. This equation can be solved numerically in a domain where H is the bottom depth and η is the water elevation height if an initial condition, $C(z,0)$ and two boundary conditions at $z = -H$ and $z = \eta$ are known. The most obvious boundary condition to apply at the end points is = 0 which is a zero flux (insulating) condition implying that no tracer is generated or destroyed within the domain and is hence conserved.

The above equation can be solved using a purely explicit method which leads to the general iteration (exemplified for a spatial grid with uniform grid spacing)

$$C_i^{n+1} = C_i^n + \frac{\Delta t}{\Delta z^2}\left[\frac{1}{2}(K_{i+1}^n + K_i^n)(C_{i+1}^n - C_i^n) - \frac{1}{2}(K_i^n + K_{i-1}^n)(C_i^n - C_{i-1}^n)\right]$$

where *n* and *i* respectively are the time and spatial (in the vertical) incremental indices and Δt and Δz are respectively the numerical time step and grid spacing. However, for stability and monotonicity of the numerical solutions, the condition needs to be satisfied which imposes a severe restriction on the time step. Therefore, an implicit method is favored and the most obvious candidate is

$$C_i^{n+1} - C_i^n - \frac{\Delta t}{\Delta z^2}\left[\frac{1}{2}(K_{i+1}^{n+1} + K_i^{n+1})(C_{i+1}^{n+1} - C_i^{n+1}) - \frac{1}{2}(K_i^{n+1} + K_{i-1}^{n+1})(C_i^{n+1} - C_{i-1}^{n+1})\right] = 0$$

which is still linear because *K* is known. However, although numerically unconditionally stable (allowing the use of any value for Δt), this method is only first order accurate in time and requires the inversion of a matrix. Hence, it was decided that the best compromise (in terms of numerical stability and order of accuracy of the method) was to use the Crank-Nicholson time discretization, which led to the scheme

$$C_i^{n+1} - \frac{1}{2}\cdot\frac{\Delta t}{\Delta z^2}\left[\frac{1}{2}(K_{i+1}^{n+1} + K_i^{n+1})(C_{i+1}^{n+1} - C_i^{n+1}) - \frac{1}{2}(K_i^{n+1} + K_{i-1}^{n+1})(C_i^{n+1} - C_{i-1}^{n+1})\right]$$
$$= C_i^n + \frac{1}{2}\cdot\frac{\Delta t}{\Delta z^2}\left[\frac{1}{2}(K_{i+1}^n + K_i^n)(C_{i+1}^n - C_i^n) - \frac{1}{2}(K_i^n + K_{i-1}^n)(C_i^n - C_{i-1}^n)\right]$$

and it is unconditionally stable and second-order accurate in time and space. However, in order to maintain numerical accuracy, sufficiently small Δt and Δz values need to be employed. The inversion of the resulting tri-diagonal matrix can be done in a highly efficient manner thus minimizing the computational cost of solving the above equation.

5.2 Lagrangian Particle Path Tracking Approach

For a given viscosity/diffusivity coefficient, $K(z,t)$, mass-less and point-like particles which are devoid of momentum and friction and behavior (e.g. swimming, etc.) are transported around via a random walk mechanism (Chandrasekhar, 1943). Therefore, in one-dimension, with a spatio-temporally constant viscosity/diffusivity coefficient, K_0, a particle which begins at a spatial location z^0, will end up at a location z^1 after a time interval, Δt where

$$z^1 = z^0 + r\cdot\sqrt{2K_0\Delta t}$$

where *r* is a random number in the interval [-1,1]. This leads to the general first-order accurate Euler iteration

$$z^{n+1} = z^n + r \cdot \sqrt{2K(z^n, t^n)\Delta t}$$

and, a second-order accurate Runge-Kutta iteration

$$z^{n+1} = z^n + r \cdot \sqrt{2K\left(z^n + \tfrac{1}{2}\delta z, t^n + \tfrac{1}{2}\Delta t\right)\Delta t} \quad ; \delta z = \sqrt{2K(z^n, t^n)\Delta t}$$

Therefore, this particle path iteration can be applied in the vertical to the western Lake Erie set-up using the eddy-viscosity resulting from the ROMS simulations provided that a set of initial particle locations for the full ensemble $\{z^0\}$ is known.

5.3 **Passive Tracer and Particle Path Tracking Results and Discussion**

Using an initial tracer and particle distribution within the top two meters of the water column (which is where scum usually resides) a series of passive tracer and Lagrangian particle path simulations were carried out in a Matlab environment. For the tracer, the active regions had a value of 1.0 and the background/ambient value was set to 0.0. For the particles, 100 particles were distributed evenly in space in the vertical. The discrete tracer diffusion equations given in Section 5.1 were solved on the ROMS native vertical σ-grid itself. The particle path tracking was conducted using the second-order Runge-Kutta algorithm. The spatio-temporal eddy-viscosity field employed in these experiments was that resulting from use of the Mellor-Yamada 2.5 scheme.

The simulations were carried out for three eddy-viscosity spatio-temporal scenarios: (i) an average condition containing regions of high, low and moderate viscosity values, (ii) a low condition containing mostly low values of viscosity with intermittently occurring high values (diurnal pulses due to the meteorological forcing), and (iii) a high condition where the viscosity is consistently high in both space and time. The eddy-viscosity plots corresponding to these conditions are given in Figures E1-E3 (top panels) in Appendix E.

The results of the numerical simulations are given in figures E1-E3 of appendix E and each figure consists of a spatio-temporal plot of the eddy-viscosity (top panel), a spatio-temporal plot of the passive tracer evolution (middle panel) and a plot of the Lagrangian particles in time and space (bottom panel). Figure E1 shows that right from the beginning, the eddy-viscosity (~10^{-4} m^2/s) begins to dilute the tracer in time and space but upon encountering the region of high viscosity around day 257.0, the tracer become almost fully diluted within the top 3m of the water column. Thereafter, the tracer maintains the vertical stratification in time as there are no incursions by the eddy-viscosity in to the water

column deeper than ~3m. The Lagrangian particles too begin mixing slowly within the water column from the beginning, but upon encountering the high viscosity region around day 257.0 the mixing is exacerbated, and this is also true within the top 2m of the water column for the high viscosity regions during days 258-259. The pronounced mixing is shown by regions (within the top 3m of the water column) devoid of particles (or their dispersal) and its lack is shown by regions with particle accumulation/stagnation (of lack of movement) – for example, the region encompassing depths of 3-5 m during days 257.5-259.0.

Figure E2 shows that during the first day, the tracer begins to evolve slowly in time and space but upon encountering the region of high viscosity around day 236.5, it experiences heavy mixing in time and depth both of which reflect the temporal (~0.25 days) and spatial (vertical, ~5m) extents of the viscosity region (top panel). Thereafter, the tracer field remains more or less invariant in time until day 237.25 when it encounters the second high viscosity patch where it mixes further in time and space until it is almost completely uniform in value within the first ~5m of the water column. The simulated particle plot closely reflects the observations made regarding the spatio-temporal evolution of the tracer and the action of the eddy-viscosity is clearly seen. It is seen, in particular, in the rapid dispersal of the particles within the top 5m due to the action of the two high viscosity regions and the stagnation of the particles after day 236.5 between 5.0m and 6.5m due to the presence of very low viscosity values.

The tracer diffuses rapidly throughout the water column in Figure E3 and maintains this state due to the high eddy-viscosity values which are prevalent within much of the water column and also for much of the time. A theoretical estimate for a fully-mixed mean value would be where H is the bottom depth, η is the water elevation and $C(z,0)$ is the tracer initialization field. For the present application, this mean the value is 0.26 which is indeed the value indicated in the tracer plot. The Lagrangian particle plot closely reflects the tracer plot in that particles have rapidly dispersed away in the water column due to the action of the high viscosity and have accumulated at its top and bottom extremeties where the eddy-viscosity is at its ambient value of 1×10^{-8} (for the Mellor-Yamada model).

Therefore, the above numerical experiments have shown how a passive tracer and Lagrangian particle tracking approach can be employed to demonstrate how vertical eddy-viscosity brings about vertical mixing within a water column. They correctly predict that when the viscosity values are large, rapid mixing of the tracer and dispersal of the particles occur and when the viscosity values are small, the tracer maintains its stratification characteristics in depth and time and the particles exhibit stagnation/accumulation. The Matlab tracer and particle tracking tools employed here are sufficiently general in that they can be used with any time-evolving, one-dimensional viscosity field.

6.0 **Summary and Conclusions**

Cyanobacterial blooms result in surface scum layers when depleted of carbohydrates (overnight). Such scum layers are seen in Lake Erie. The bacterial cells, although variably buoyant, do not have a swimming capability and are distributed within the water column due to the action of eddy viscosity. This eddy-viscosity is generated primarily by meteorological forcing over the shallow lake bathymetry. In order to understand how it is produced, its nature and to study its dispersive effects, a one-dimensional, ROMS-based, numerical ocean modeling set-up was constructed and tested.

This set-up was also designed to have a high degree of portability in that it could be easily applied to any open water body using the following as inputs : a set of T and S initialization profiles, a representative bathymetric depth value, a representative Coriolis parameter (based on the latitude) and a fixed-point, time-series of meteorological variables to impose surface wind stresses and the net heat flux.

In order to isolate the most reasonable choices for model open boundary conditions, vertical eddy-viscosity scheme(s) and Jerlov light attenuation parameter, a series of model calibration exercises were conducted on the west Florida shelf. The horizontal grid was a 9 x 9 curvilinear, orthogonal grid and in the vertical, a terrain-following σ-grid with 20 model levels was employed. The bathymetry was a constant 10 m flat bottom, the initialization profiles for T and S were idealized, while quasi-analytical conditions and meteorological forcing variables were from NARR. These experiments indicated that the best choices for open boundary conditions were the wall/closed conditions, the vertical eddy-viscosity schemes were the Mellor-Yamada 2.5 and GLS k-ω schemes (giving comparable results), and for light attenuation, a Jerlov number of one. The Mellor-Yamada 2.5 scheme however had a much lower background viscosity level than that for the GLS schemes in the way they are implemented within ROMS.

Using this model configuration, the vertical mixing modeling set-up was applied to western Lake Erie. The horizontal and vertical grids were similar to those in the calibration set-up but now a bathymetric depth value and a Coriolis parameter representative of this geographical region were employed. The initial conditions for temperature were derived from observations and salinity was zero as the lake is purely fresh. The meteorological forcing variables were observations from the NDBC Marblehead, OH station and the radiation fluxes were from NARR. As in the calibration runs, here too the modeling set-up was always numerically stable and stability was monitored via the CFL parameter. With the exception of the vertical eddy-viscosity fields, the other physical fields generated using the Mellor-Yamada 2.5 and GLS k-ω schemes were extremely similar. The model set-up was validated by comparing the predicted surface and bottom temperatures with observations which agreed to within 1 ^{o}C and 0.5 ^{o}C respectively. An examination of the Péclet/Reynolds number showed that the modeled vertical

dynamics of western Lake Erie were driven by viscous/diffusive processes as opposed to inertial/advective processes.

Finally, using the main output from this modeling set-up – the vertical eddy-viscosity, a series of passive tracer and Lagrangian particle path tracking experiments were conducted (in Matlab) in order to examine how scum forming cyanobacteria would respond to vertical mixing. They correctly predicted the large and rapid mixing associated with the high viscosity values and the stagnation/accumulation associated with the low values. These Matlab tools are sufficiently general in that they can be employed with any time-evolving, one-dimensional field of vertical eddy-viscosity to study tracer/particle dispersal situations.

In terms of future directions and model set-up improvements: (i) the 20% reduction factor in net shortwave radiation flux correction is worth refining depending on the availability of observations (to improved model-observation comparisons for temperature), (ii) the duration for which hindcasts remain valid and any depreciation in the quality of the results should be examined, and (iii) further model-observation comparisons could be performed using additional data sets for Lake Erie and also at other water bodies (after configuring and applying the model set-up for those water bodies) to test model reliability and robustness.

Acknowledgments

The authors wish to acknowledge the financial support provided by National Center for Environmental Health at the Centers for Disease Control and Prevention (CDC) and also for the managerial support provided by Dr. Frank Aikman III of NOAA/NOS/OCS/CSDL and Mr. John D. Christensen of NOAA/NOS. Steve Ruberg of GLERL provided the validation dataset. Juli Dyble and Brian Kinlan provided insightful review to the manuscript.

References

Berliand, M. E. and Berliand, T. G., 1952. Determining the net longwave radiation of the earth with consideration of the effects of cloudiness (in Russian), *Izv. Akad. Nauk SSSR,* Ser. Geofiz 1.

Chandrasekhar, S., 1943. Stochastic problems in physics and astronomy, *Reviews of Modern Physics*, Vol. 15, pp. 1-89.

Fairall, C.W., E.F. Bradley, D.P. Rogers, J.B. Edson and G.S. Young, 1996a: Bulk parameterization of air-sea fluxes for tropical ocean-global atmosphere Coupled-Ocean Atmosphere Response Experiment, *Journal of Geophysical Research*, Vol. 101, pp. 3747-3764.

Fairall, C.W., E.F. Bradley, J.S. Godfrey, G.A. Wick, J.B. Edson, and G.S. Young, 1996b: Cool-skin and warm-layer effects on sea surface temperature, *Journal of Geophysical Research*, Vol. 101, pp. 1295-1308.

Jackett, D. R. and McDougall, T. J., 1995. Minimal adjustment of hydrostatic profiles to achieve statistic stability, *J. of Atmos. And Oceanic Tech*., Vol. 12, pp. 381-389.

Lanerolle, L. W. J., Tomlinson, M. C., Gross, T. F., Aikman III, F., Stumpf, R. P., Kirkpatrick, G. J. and Pederson, B. A., 2006. Numerical investigation of the effects of upwelling on harmful algal blooms off the west Florida coast, *Estuarine, Coastal and Shelf Science,* Vol. 70, pp. 599-612.

Lanerolle, L. W. J., Wynne, T. T., Patchen, R. C., Tomlinson, M. C., Xu, J., Ortiz, C., Christensen, J. D., Birger, A. and Shuford, R., 2009a. Modeling the movement of harmful algal blooms (HABs) on the west Florida shelf using hydrodynamic model outputs, (*in preparation)*.

Lanerolle, L. W. J., Patchen, R. P. and Aikman III, F., 2009b. The implementation, calibration and validation of a coupled numerical ocean modeling system for the west Florida shelf, *(in preparation)*.

Lanerolle, L. W. J., Patchen, R. P. and Aikman III, F., 2009c. The second generation Chesapeake Bay Operational Forecast System (CBOFS2) : A ROMS based modeling system (Part I), *(in preparation).*

Liu, W. T., Katsaros, K. B. and, Businger, J. A., 1979. Bulk parameterization of the air-sea exchange of heat and water vapor including the molecular constraints a the interface, *Journal of Atmospheric Sciences*, Vol. 36, pp. 1722-1735.

Mellor, G. L., and Yamada, T., 1982. Development of a turbulence closure model for geophysical fluid problems, *Reviews of Geophysics and Space Physics*, Vol. 20, pp. 851-875.

North American Regional Reanalysis (NARR), 2009. http://www.emc.ncep.noaa.gov/mmb/rreanl/

Paulson, C. A. and Simpson, J. J., 1977. Irradiance measurements in the upper ocean, *Journal of Physical Oceanography,* Vol. 7, pp. 952-956.

SeaGrid, 2009. http://woodshole.er.usgs.gov/operations/modeling/seagrid/seagrid.html

Water density calculator, 2009. http://www.csgnetwork.com/h2odenscalc.html

Shchepetkin, A. F. and McWilliams, J. C., 1998. Quasi-monotone advection schemes based on explicit locally adaptive dissipation, *Monthly Weather Review*, Vol. 126, pp. 1541-1580.

Shchepetkin, A. F. and McWilliams, J. C., 2003. A method for computing horizontal pressure-gradient forcing in an oceanic model with a nonaligned vertical coordinate, *Journal of Geophysical Research*, Vol. 108, No. C3, pp 1-34.

Shchepetkin, A. F. and McWilliams, J. C., 2004. The Regional Oceanic Modeling System : a split-explicit, free-surface, topography-following-coordinate ocean model, *Ocean Modelling*, Vol. 9 (4), pp. 347-404.

.

Song, Y. T., and Haidvogel, D. B., 1994. A semi-implicit ocean circulation model using a generalized topography following coordinate system, *Journal of Computational Physics*, Vol. 115, pp. 228-244.

Styles, R., and Glenn, S. M., 2000. Modeling stratified wave and current bottom boundary layers in the continental shelf, *Journal of Geophysical Research*, Vol. 105, pp. 24119-24139.

Warner, J. C., Sherwood, C. R., Arango, H. G., and Signell R. P., 2005. Performance of four turbulence closure methods implemented using a generic length scale method, *Ocean Modelling*, Vol. 8, pp. 81-113.

Appendix A : Sensitivity to Choice of Open Boundary Conditions

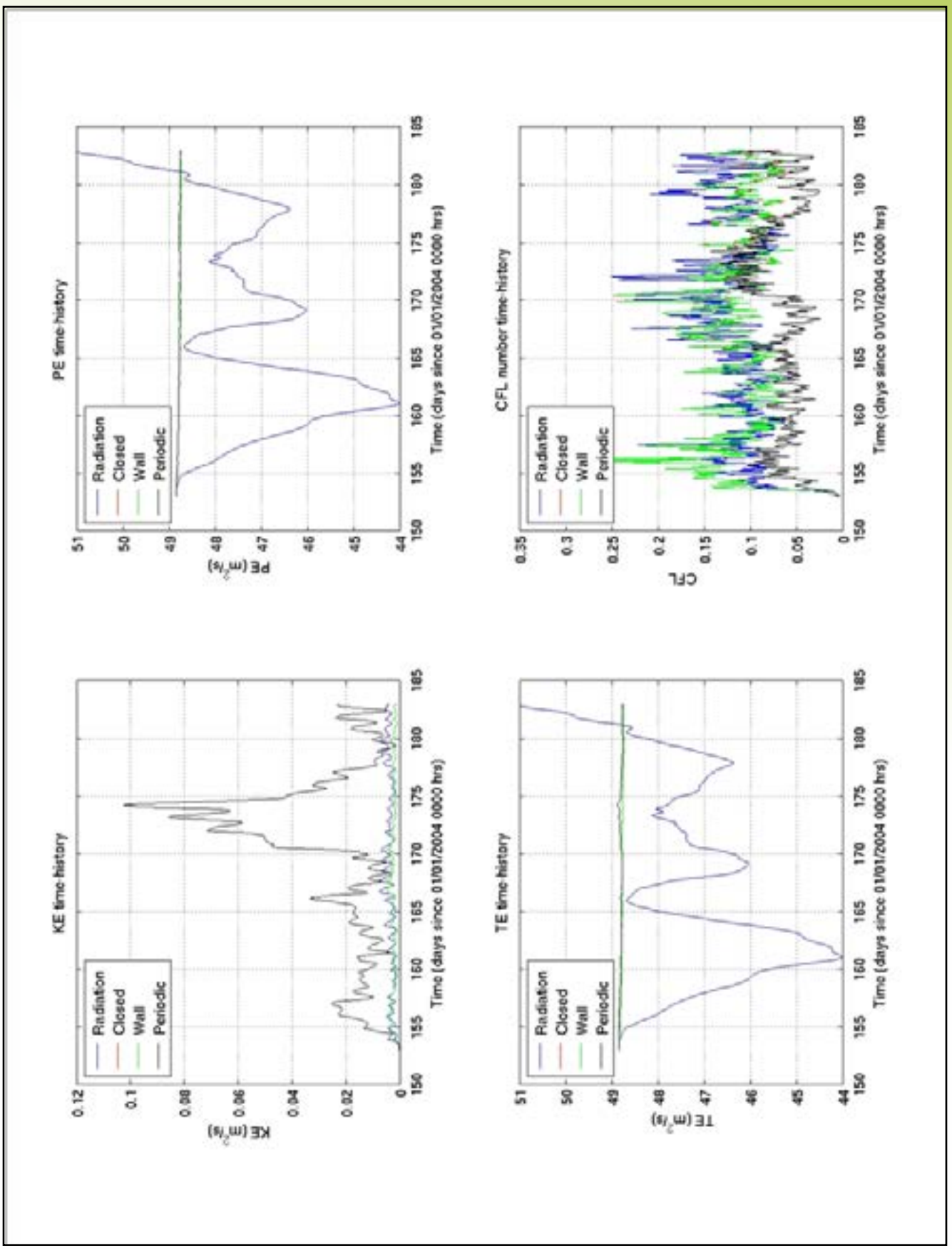

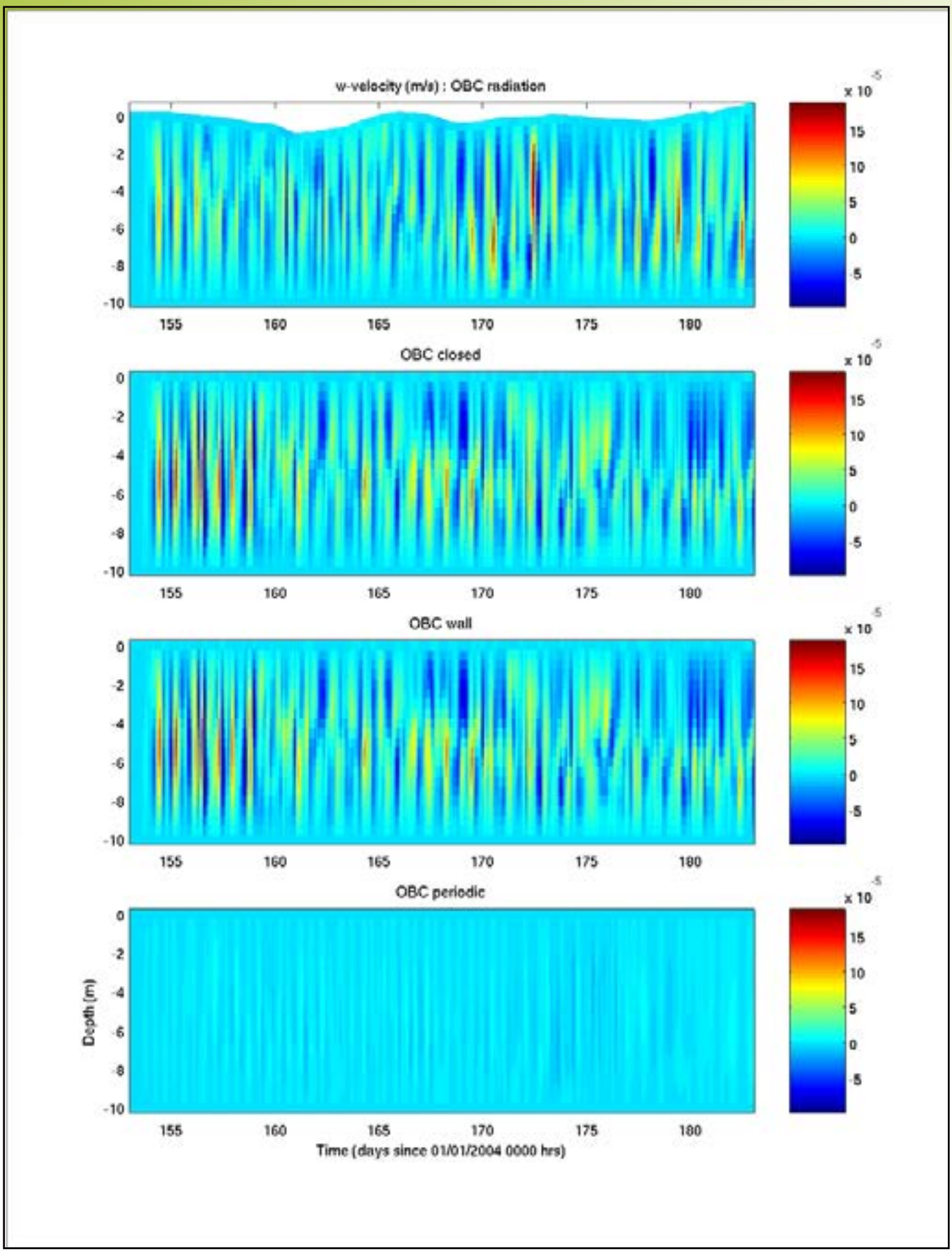

Figure A2 : Effect of open boundary conditions on the vertical (w) velocity/current.

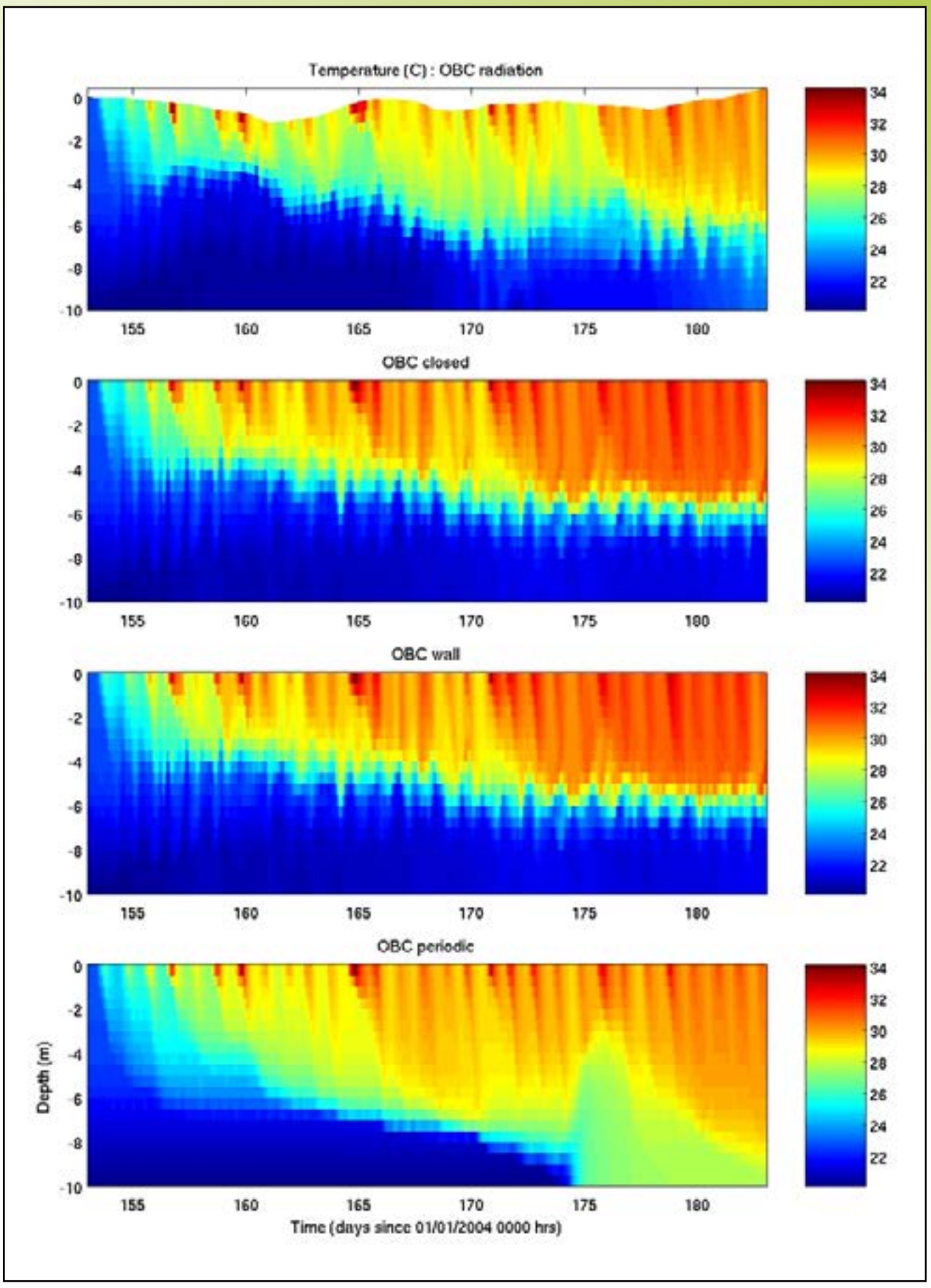

Figure A3 : Effect of open boundary conditions on the potential temperature.

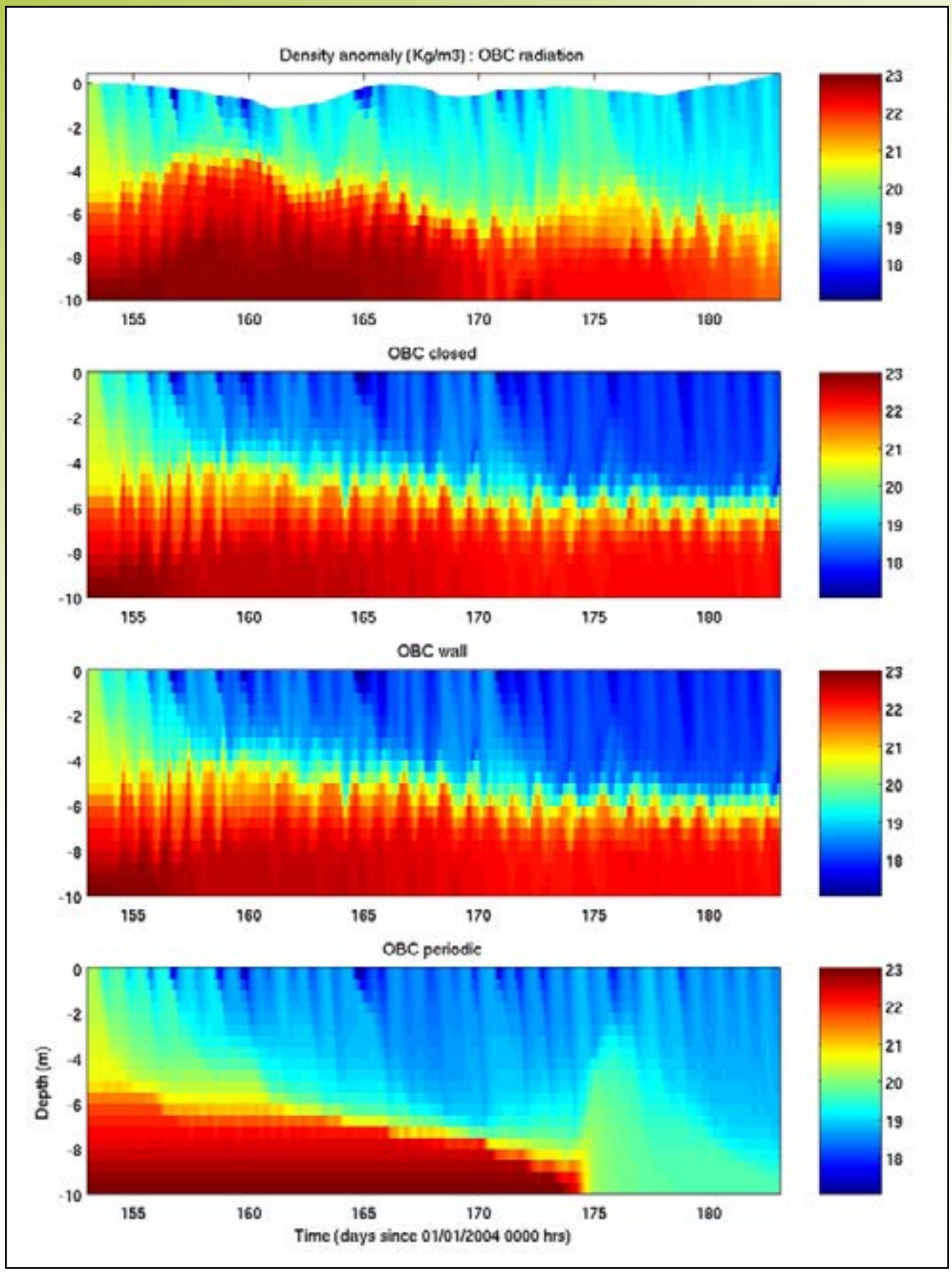

Figure A4 : Effect of open boundary conditions on the density anomaly.

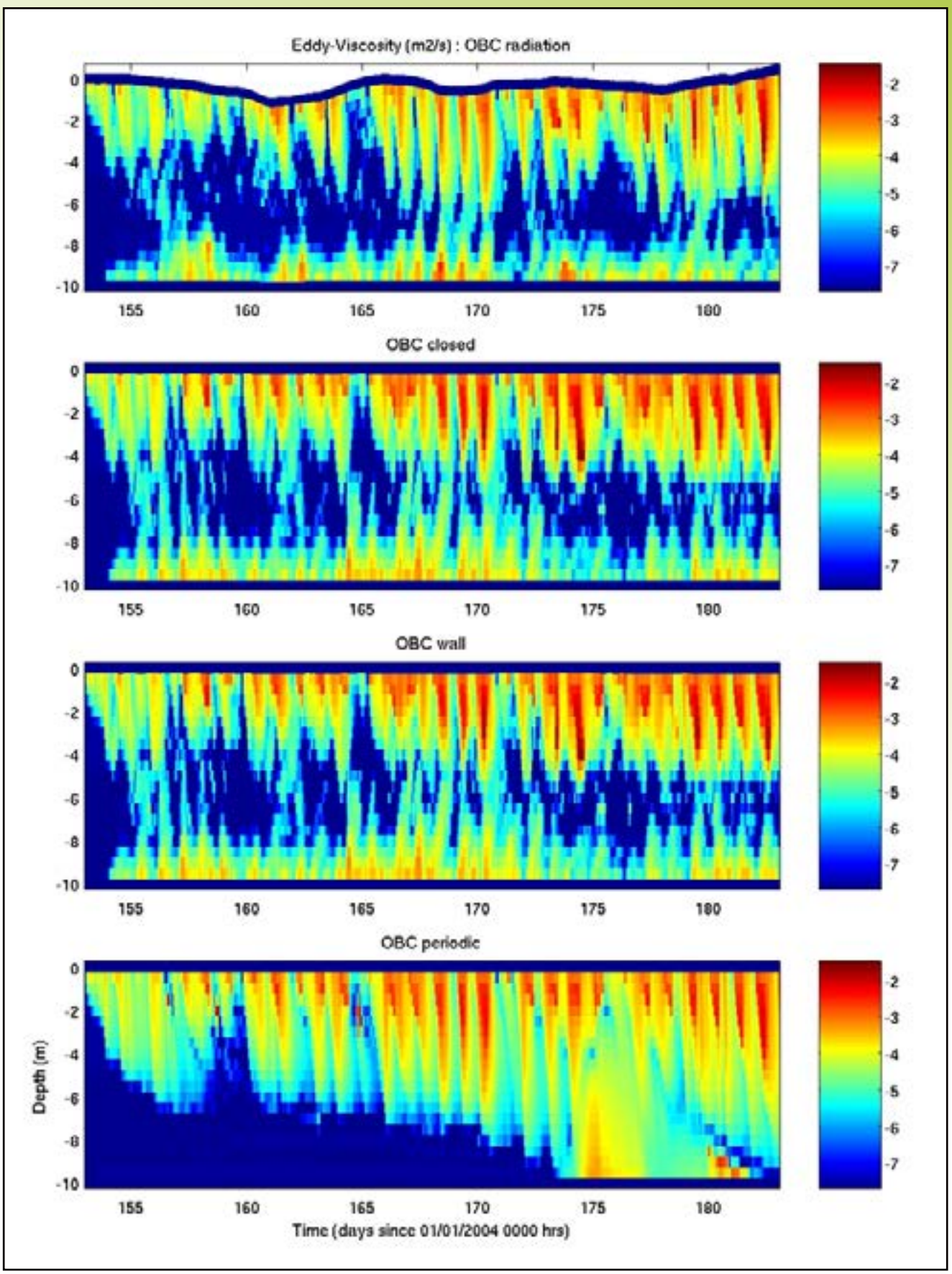

Figure A5 : Effect of open boundary conditions on the vertical eddy-viscosity.

Appendix B : Sensitivity to Choice of Vertical Eddy-Viscosity Closure Scheme

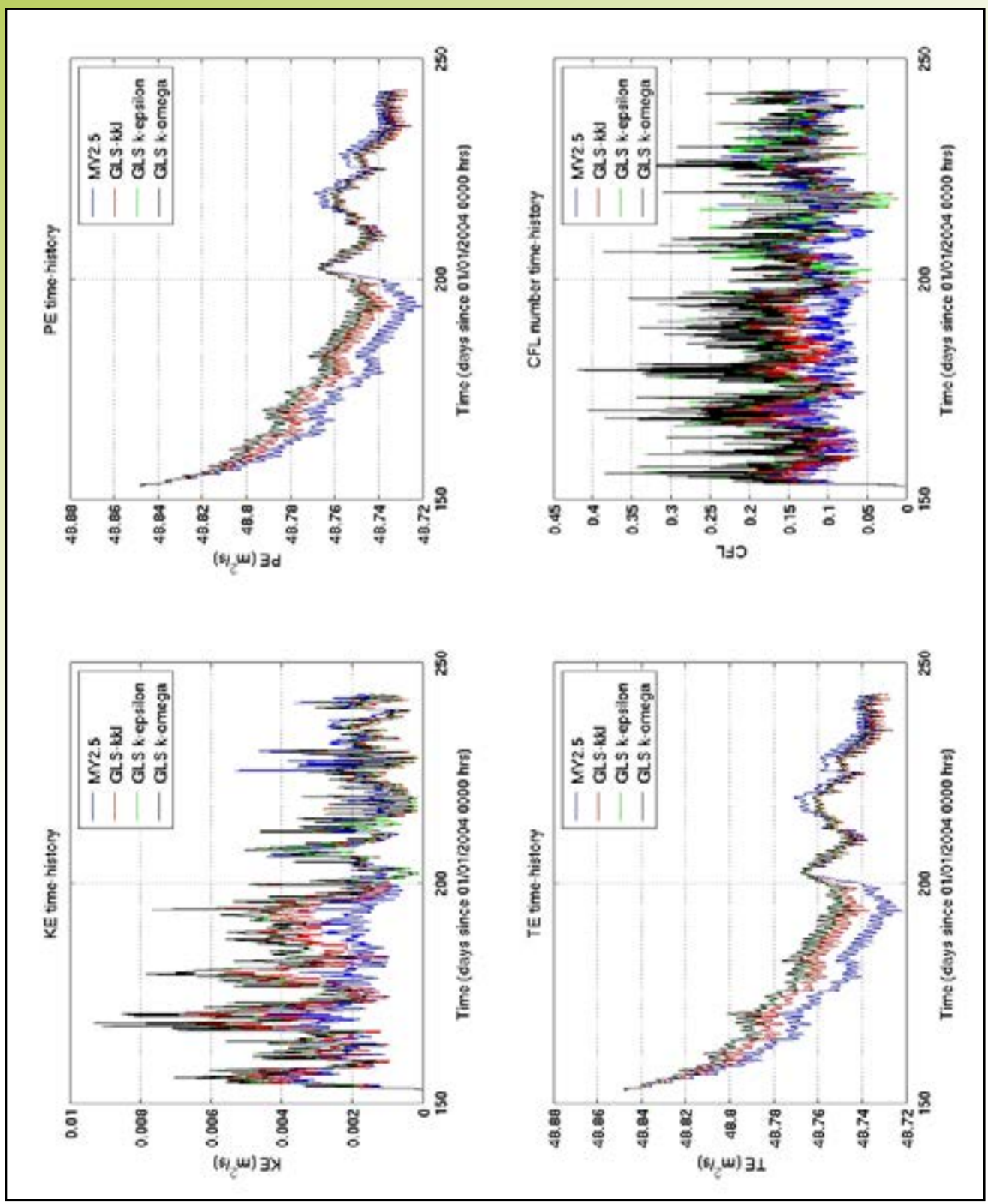

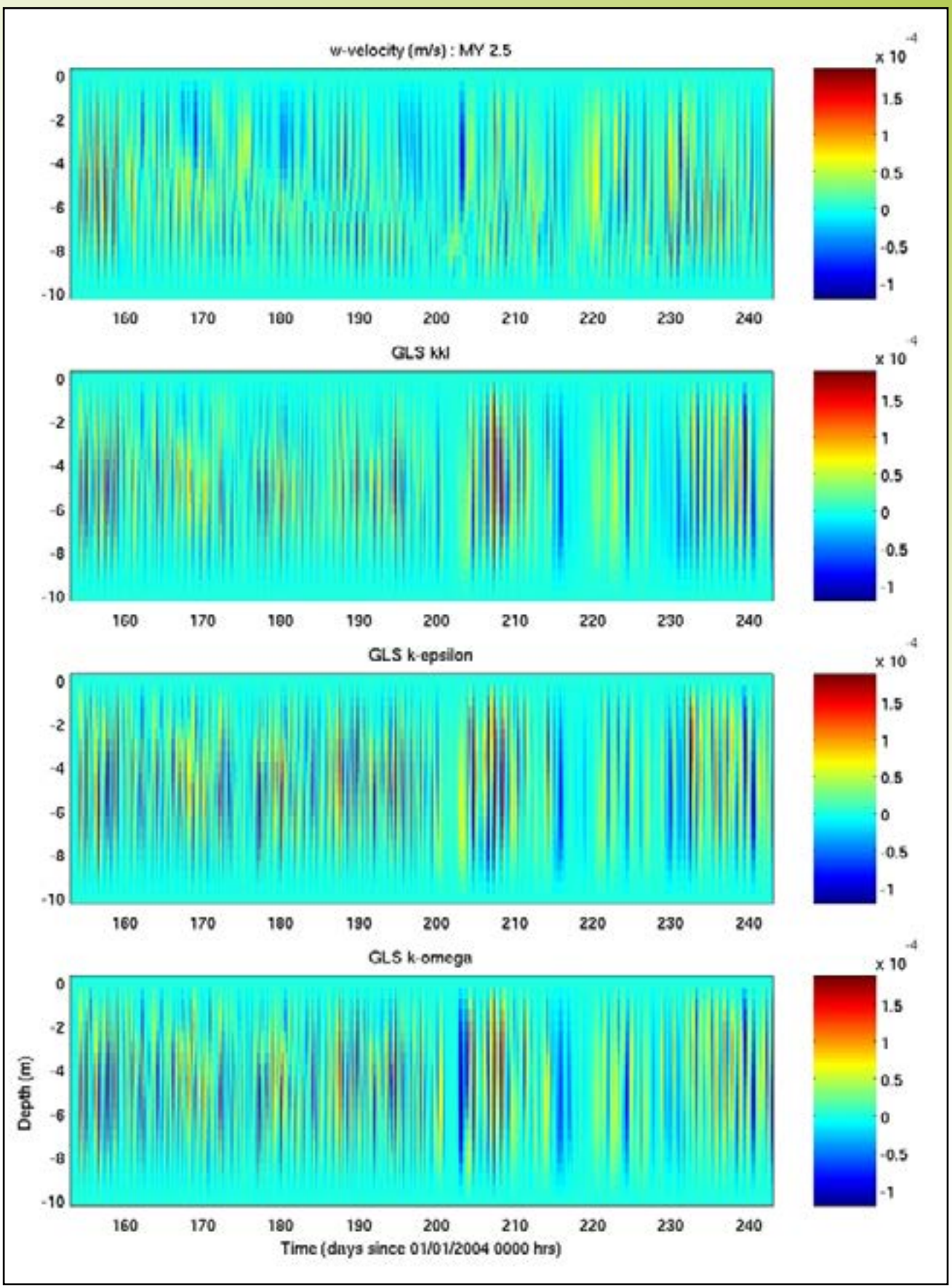

Figure B2 : Effect of vertical eddy-viscosity scheme on the vertical (w) velocity/current.

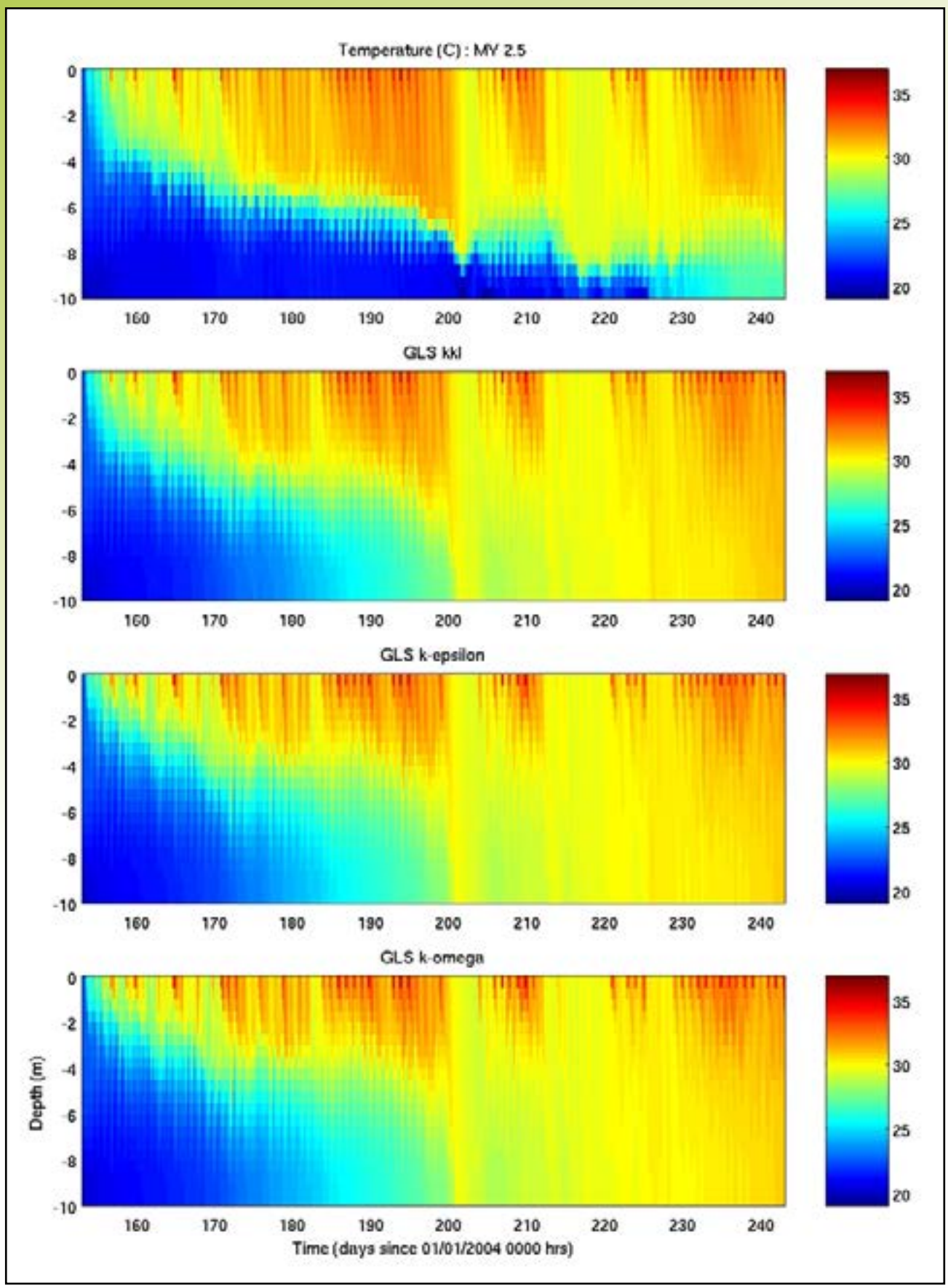

Figure B3 : Effect of vertical eddy-viscosity scheme on the potential temperature.

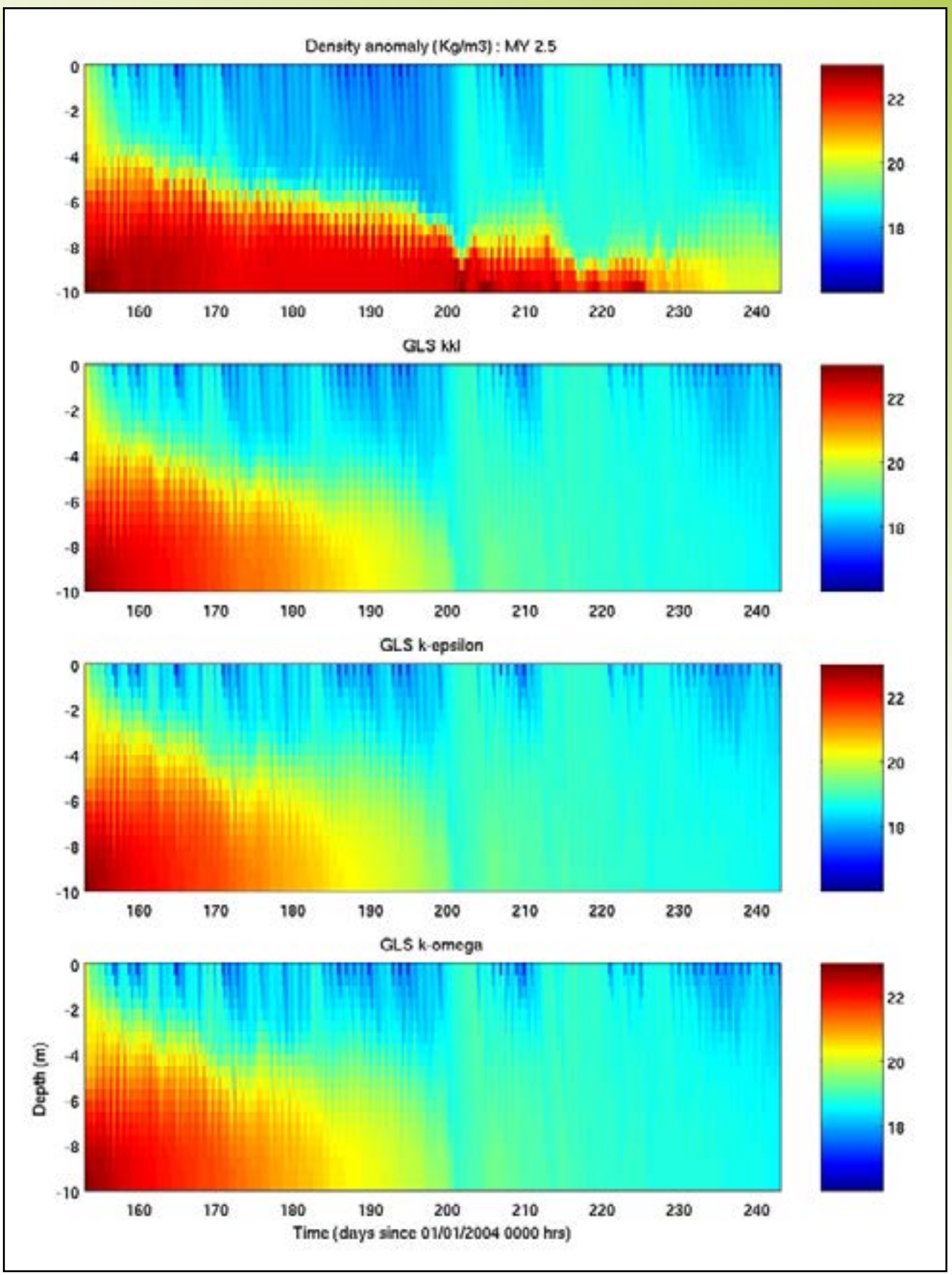

Figure B4 : Effect of vertical eddy-viscosity scheme on the density anomaly.

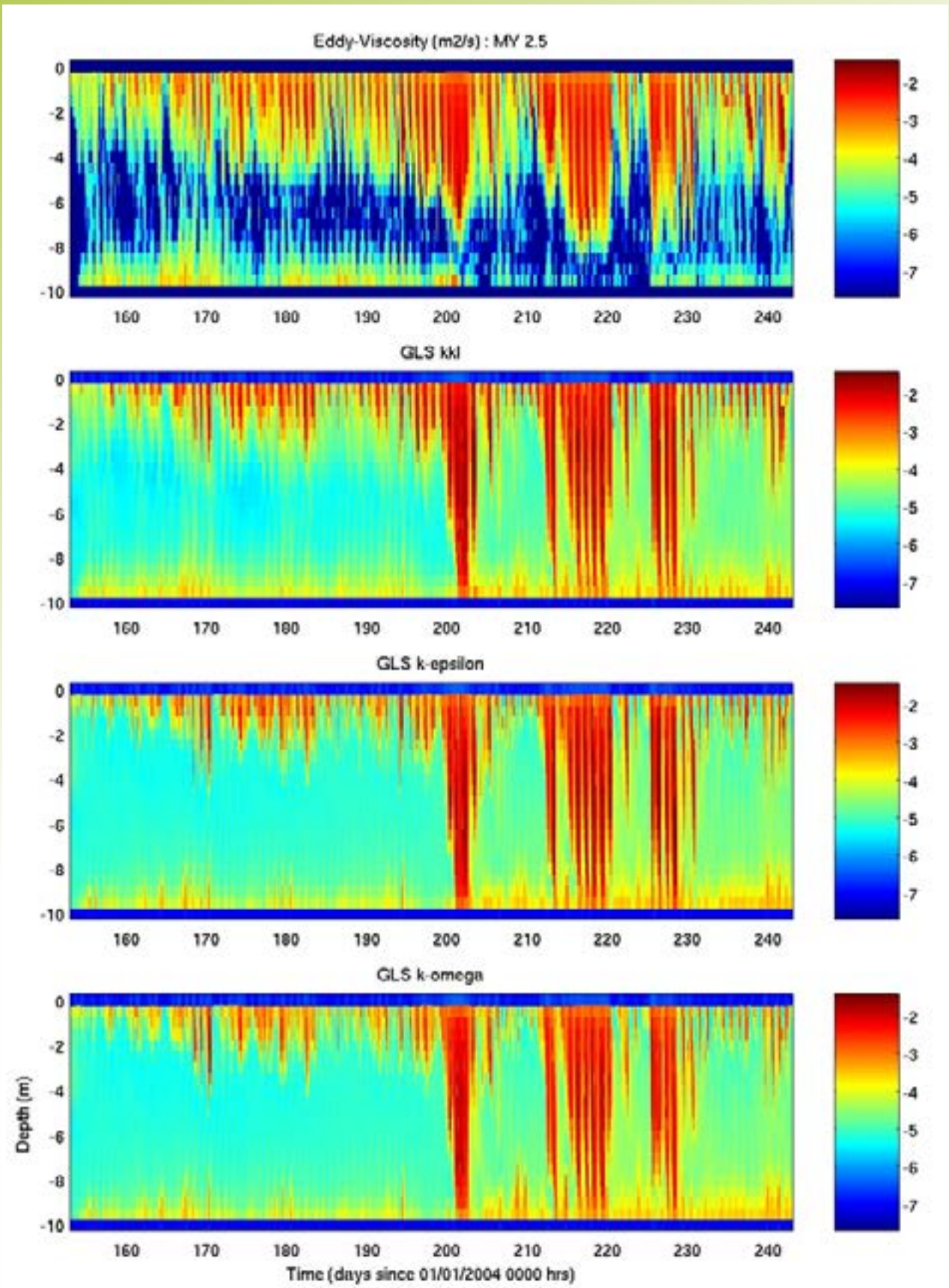

Figure B5 : The vertical eddy-viscosities resulting from the different schemes/models.

Appendix C : Sensitivity to Choice of the Jerlov Water Type

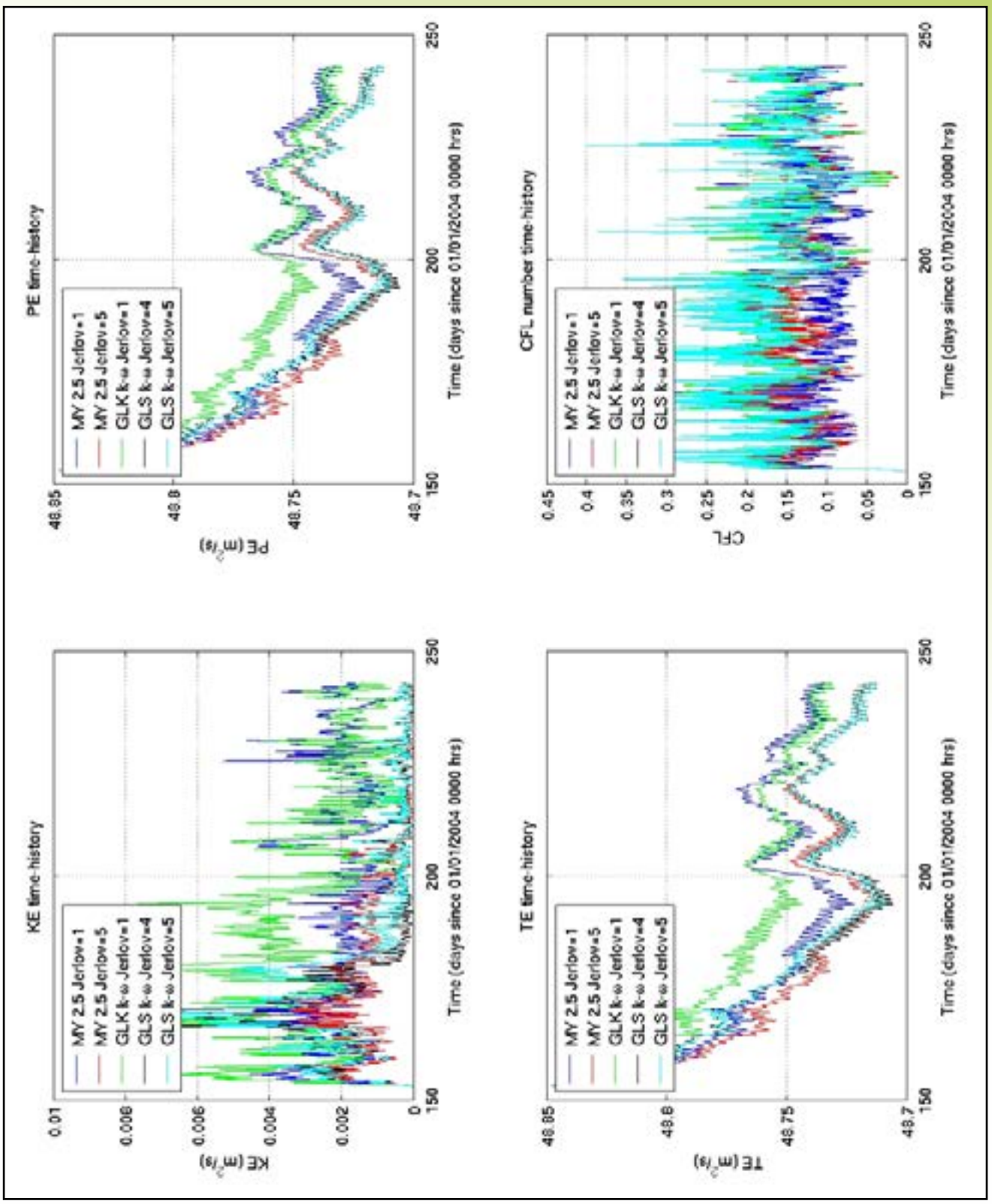

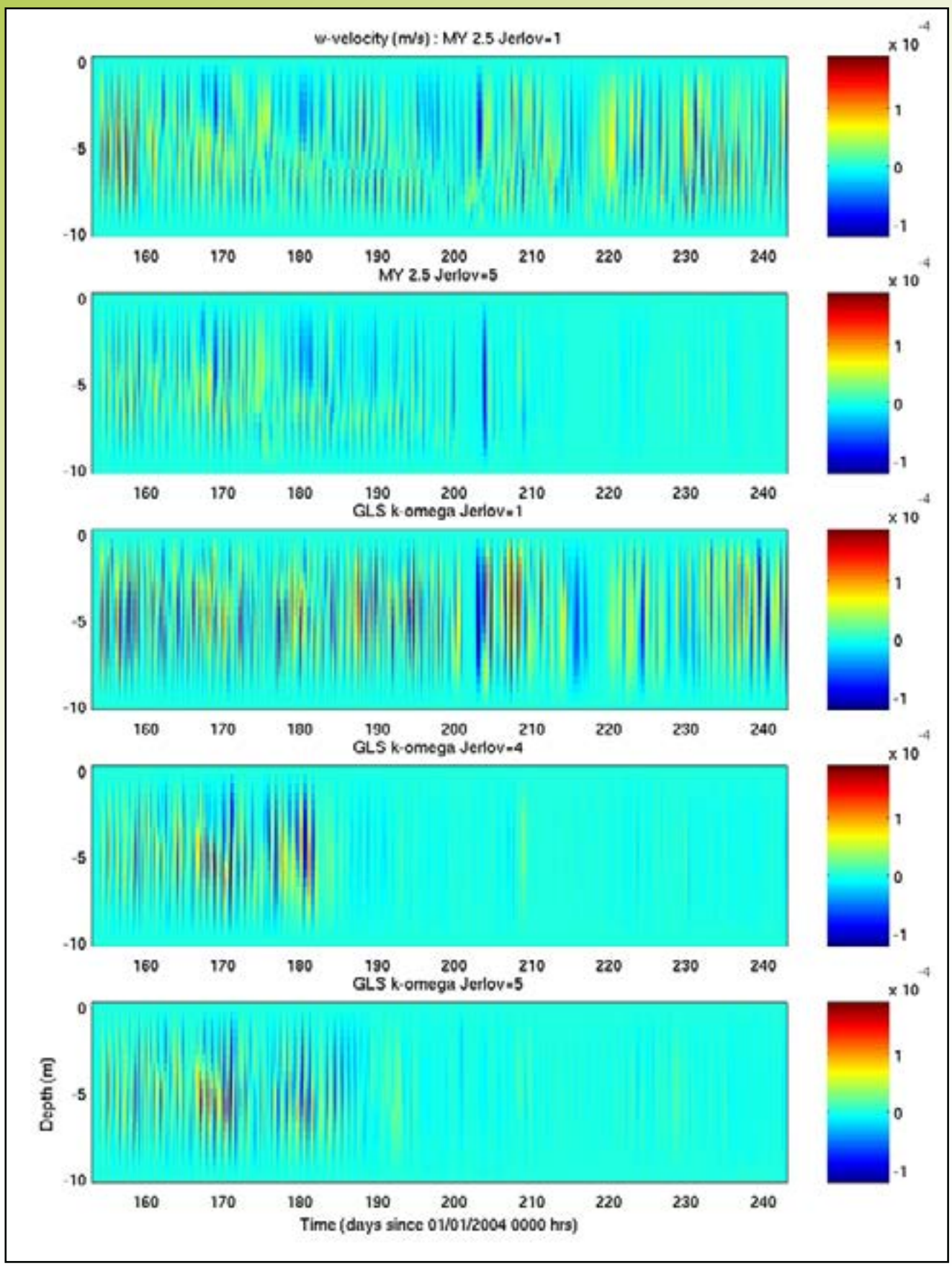

Figure C2 : Effect of the Jerlov parameter on the vertical (w) velocity/current.

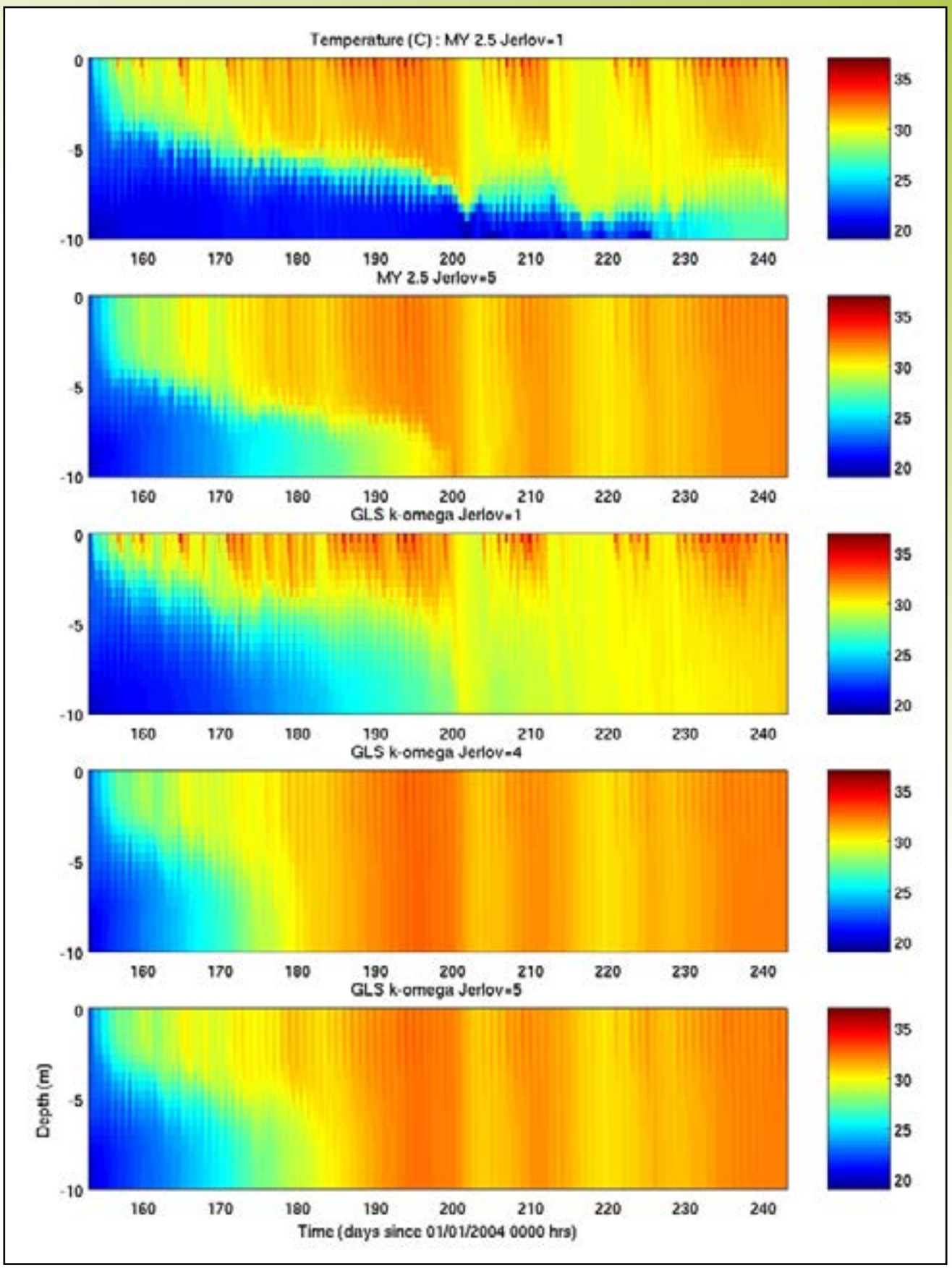

Figure C3 : Effect of the Jerlov parameter on the potential temperature.

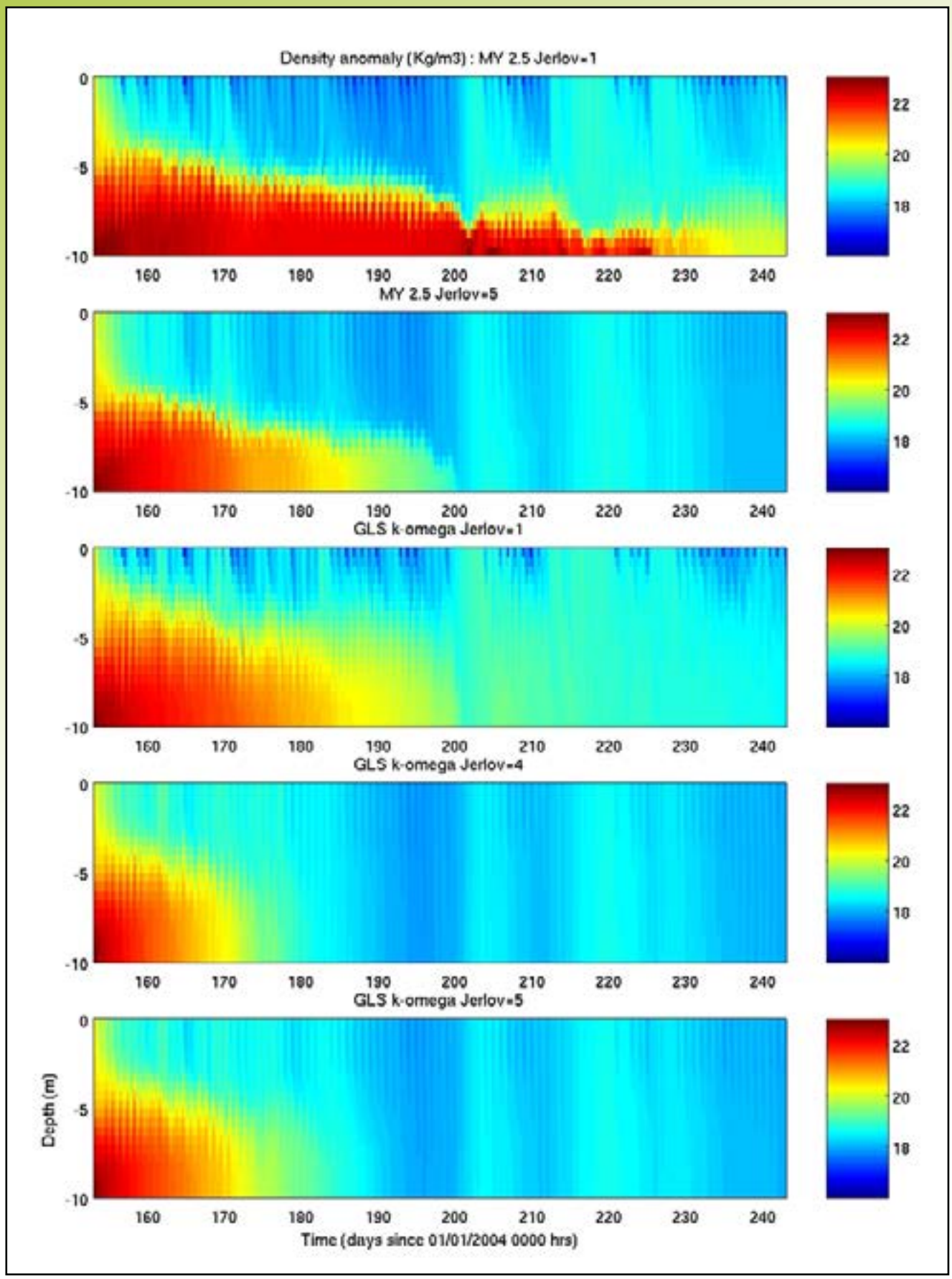

Figure C4 : Effect of the Jerlov parameter on the density anomaly.

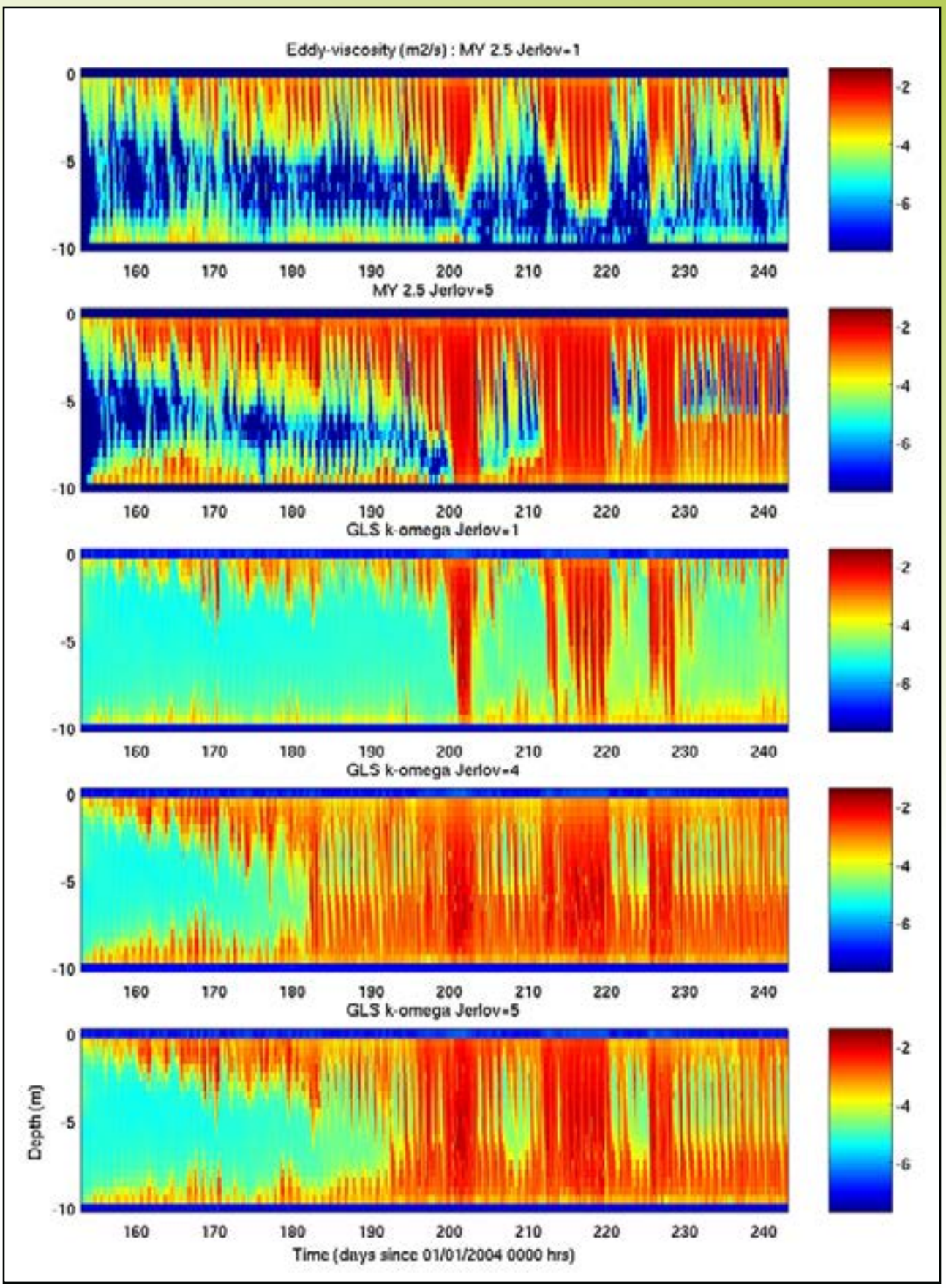

Figure C5 : Effect of the Jerlov parameter on the vertical eddy-viscosity.

Appendix D : Results for the Western Lake Erie Simulation

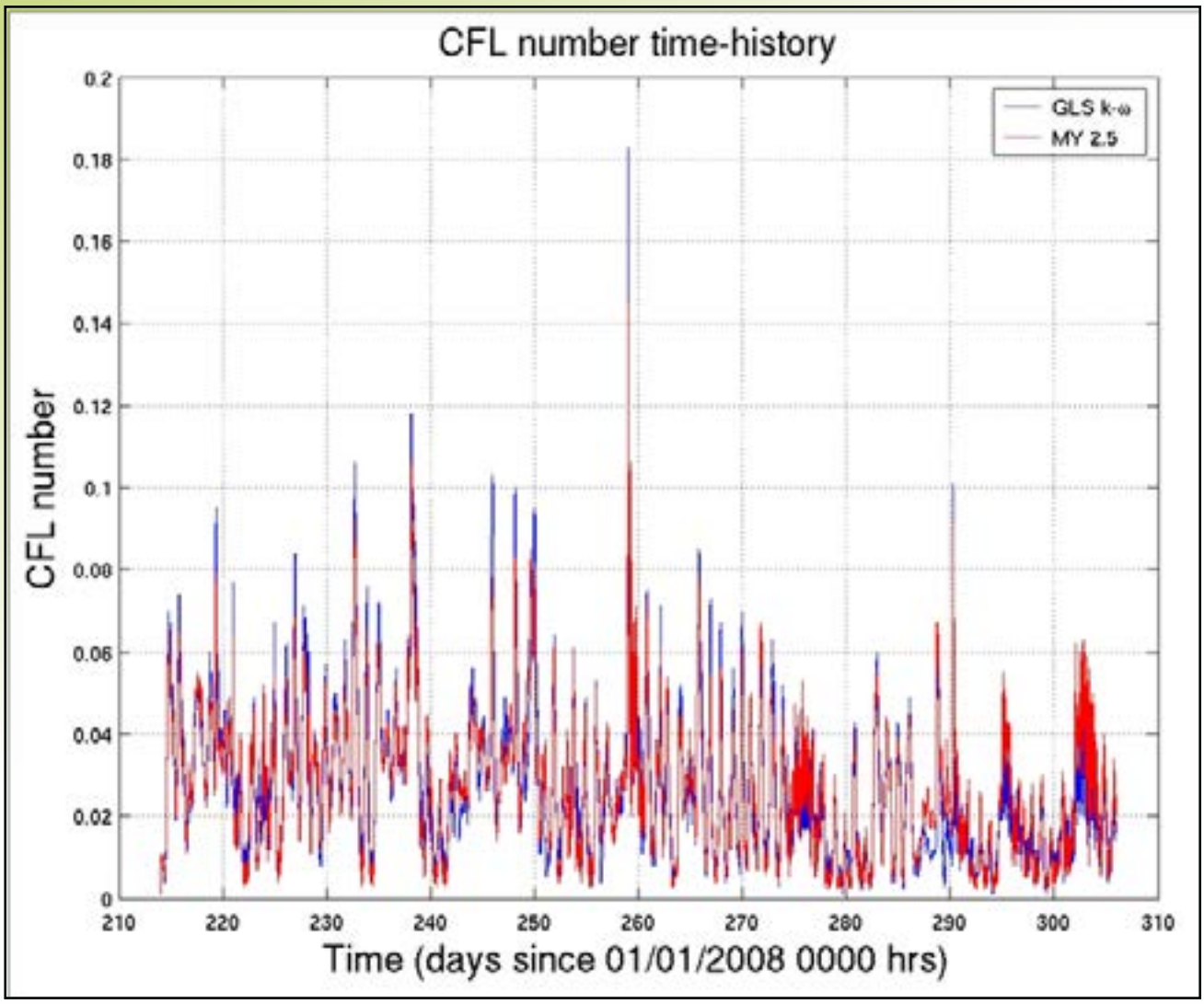

Figure D1 : CFL number time history.

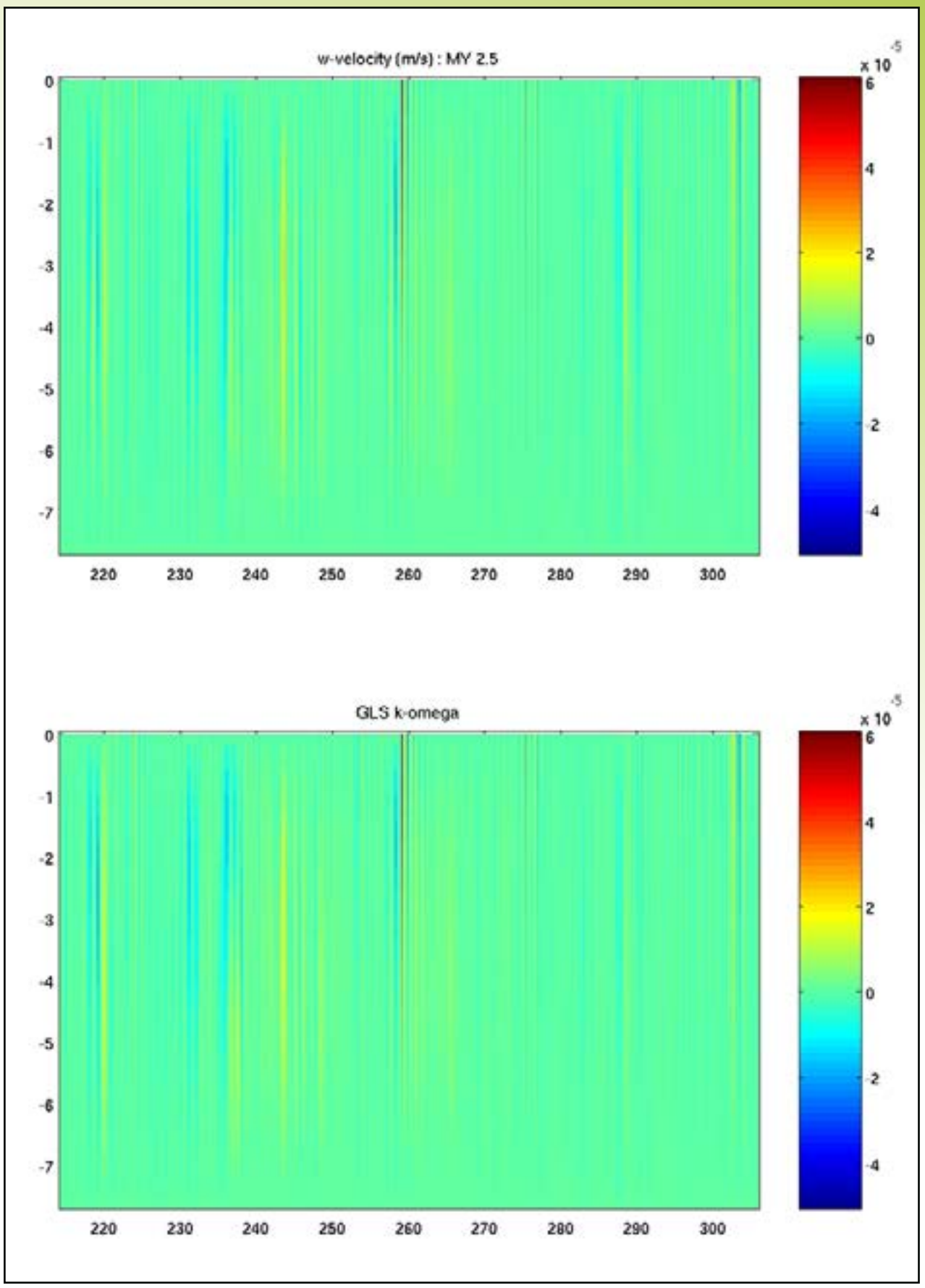

Figure D2 : Spatio-temporal evolution of the vertical w-velocity.

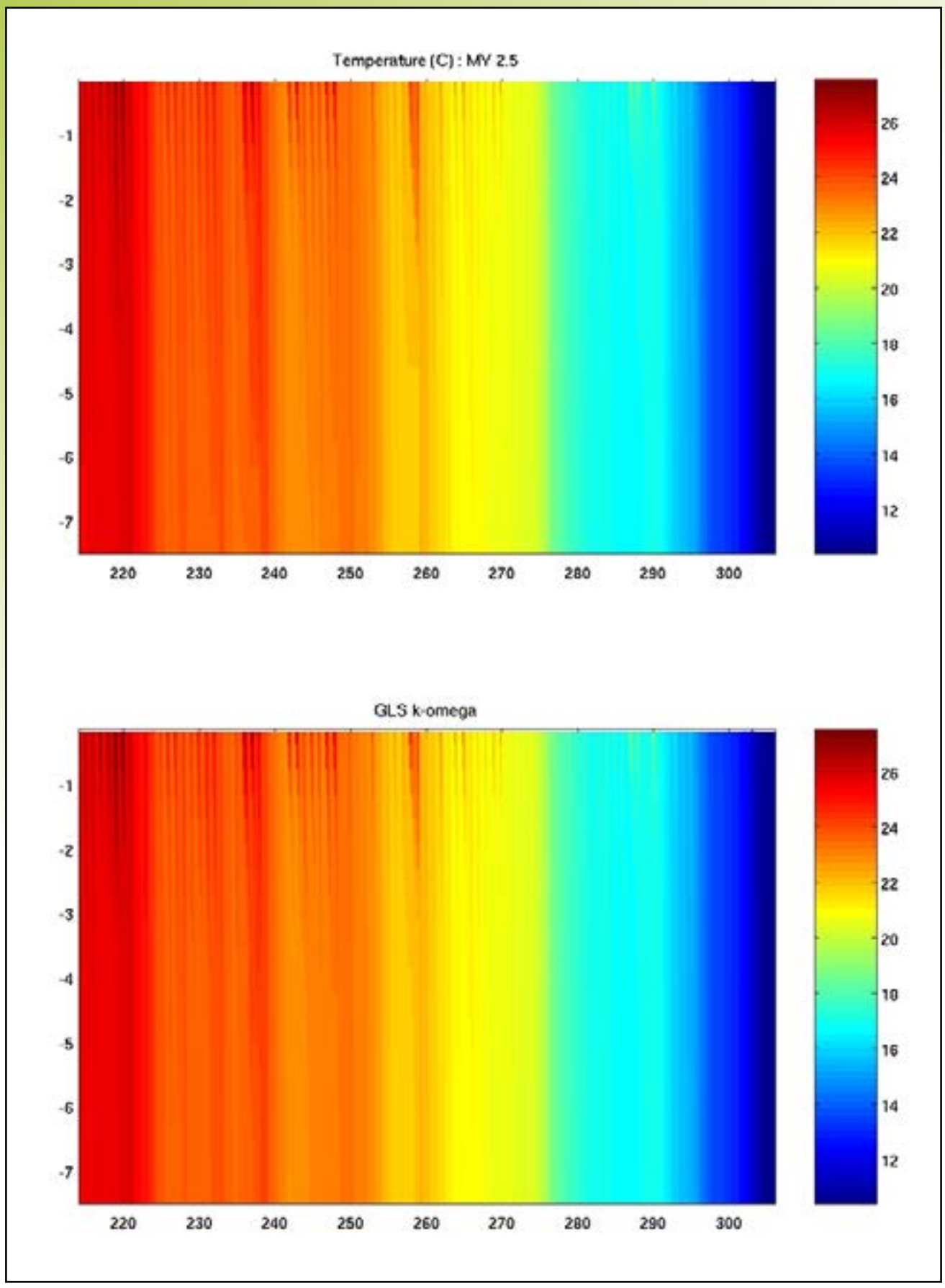

Figure D3 : Spatio-temporal evolution of the potential temperature.

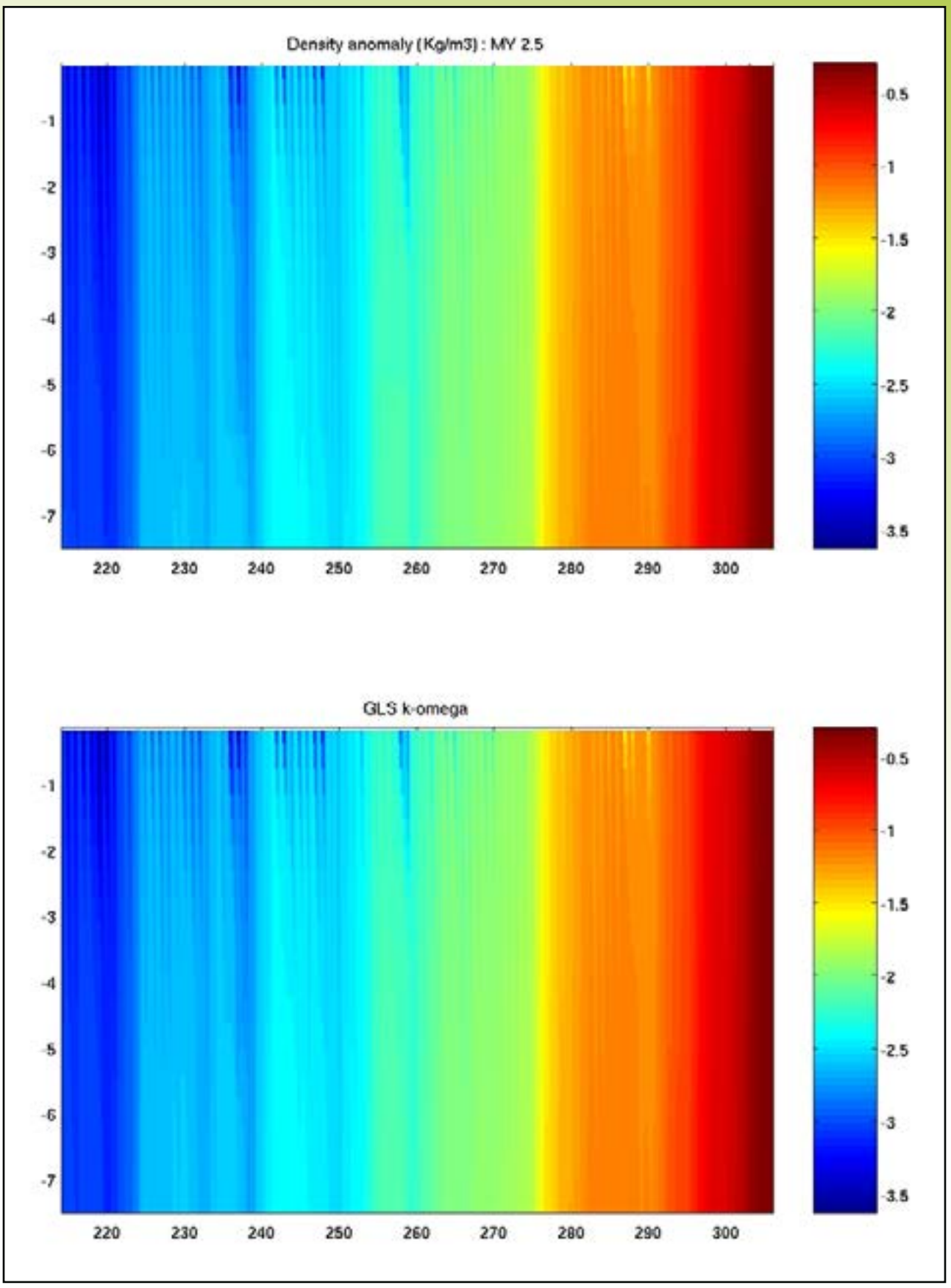

Figure D4 : Spatio-temporal evolution of the density anomaly.

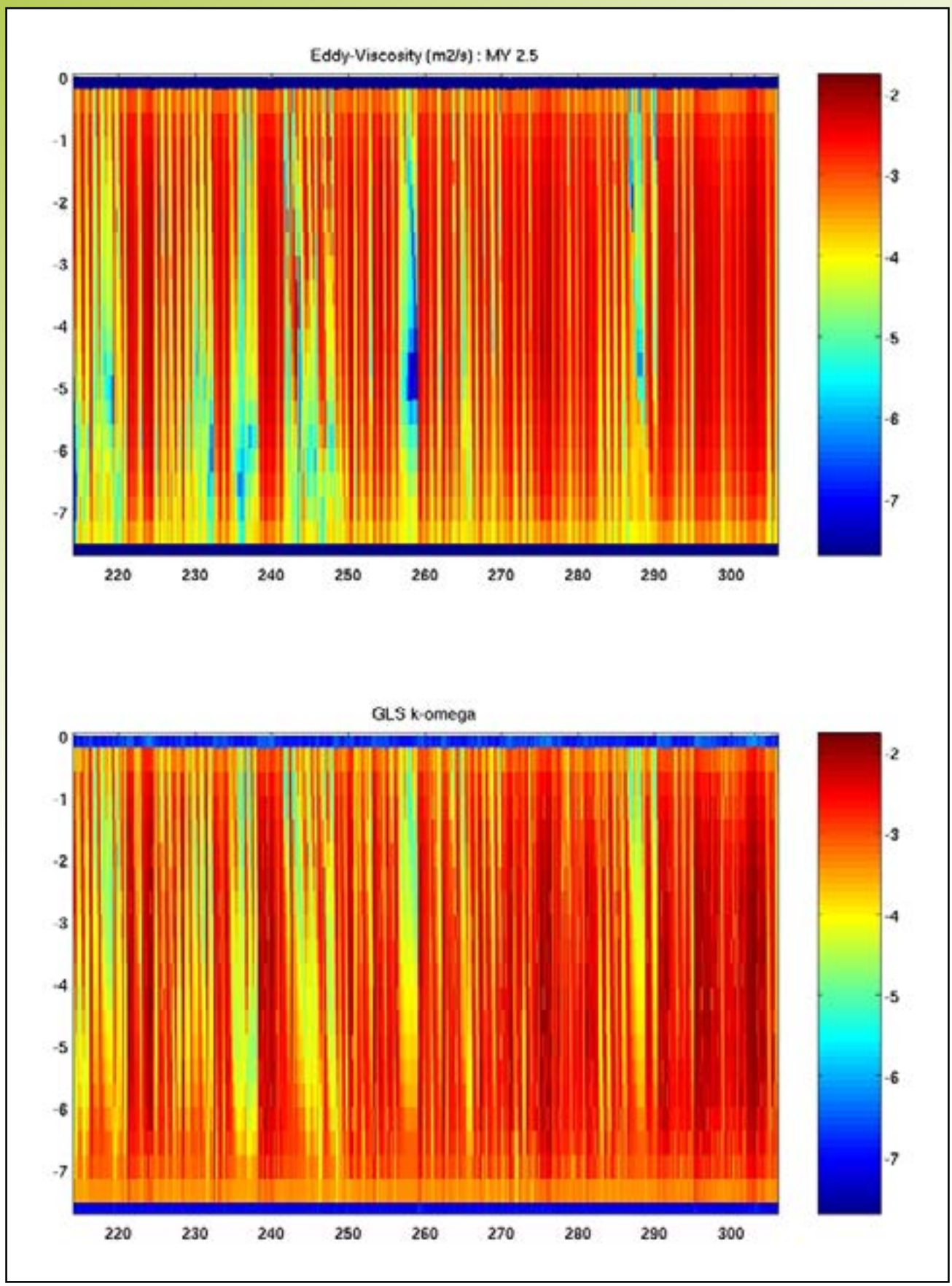

Figure D5 : Spatio-temporal evolution of the vertical eddy-viscosity.

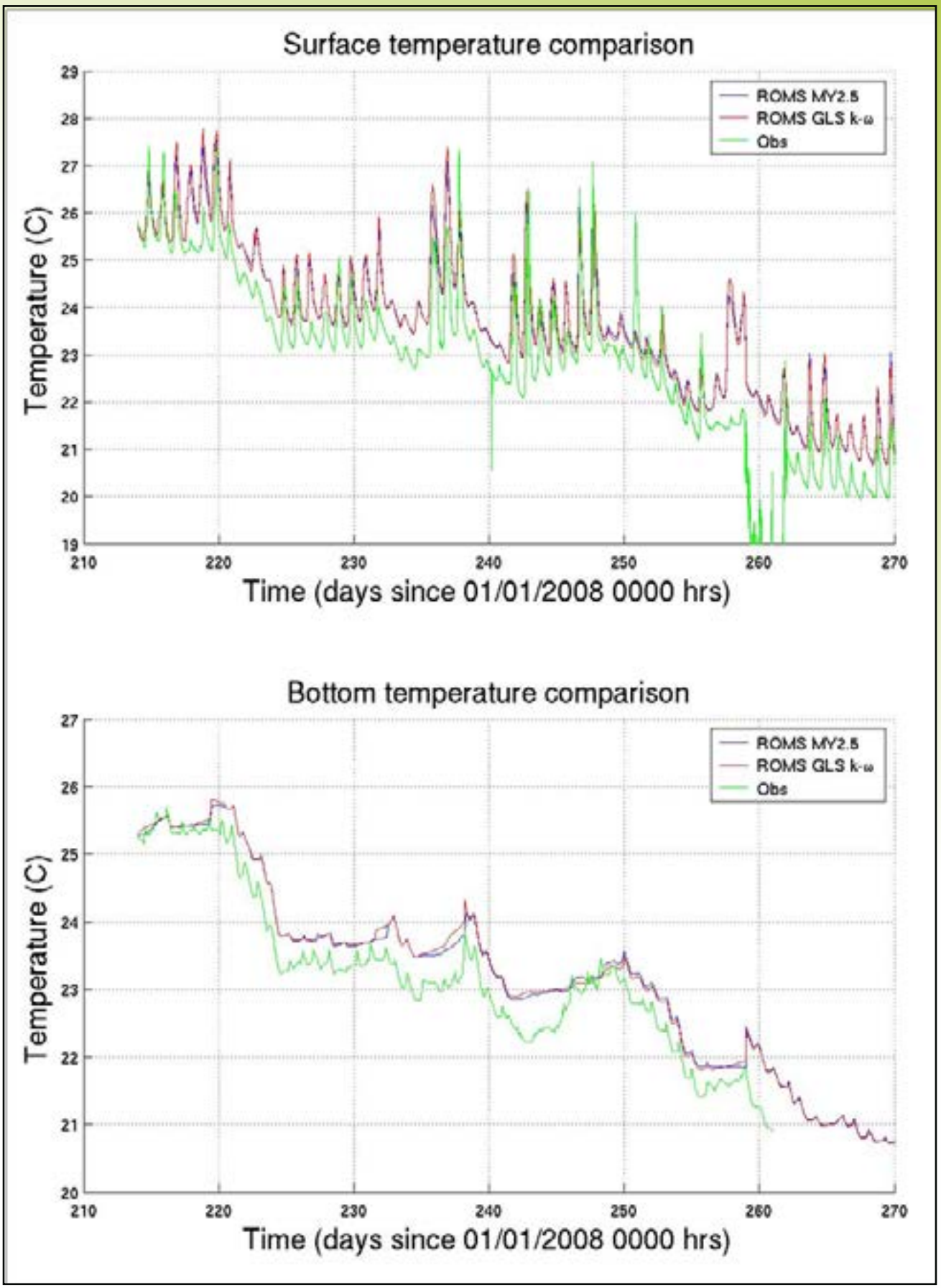

Figure D6 : Model predicted surface and bottom temperature comparison with observations.

Appendix E : Idealized Vertical Mixing Numerical Experiments

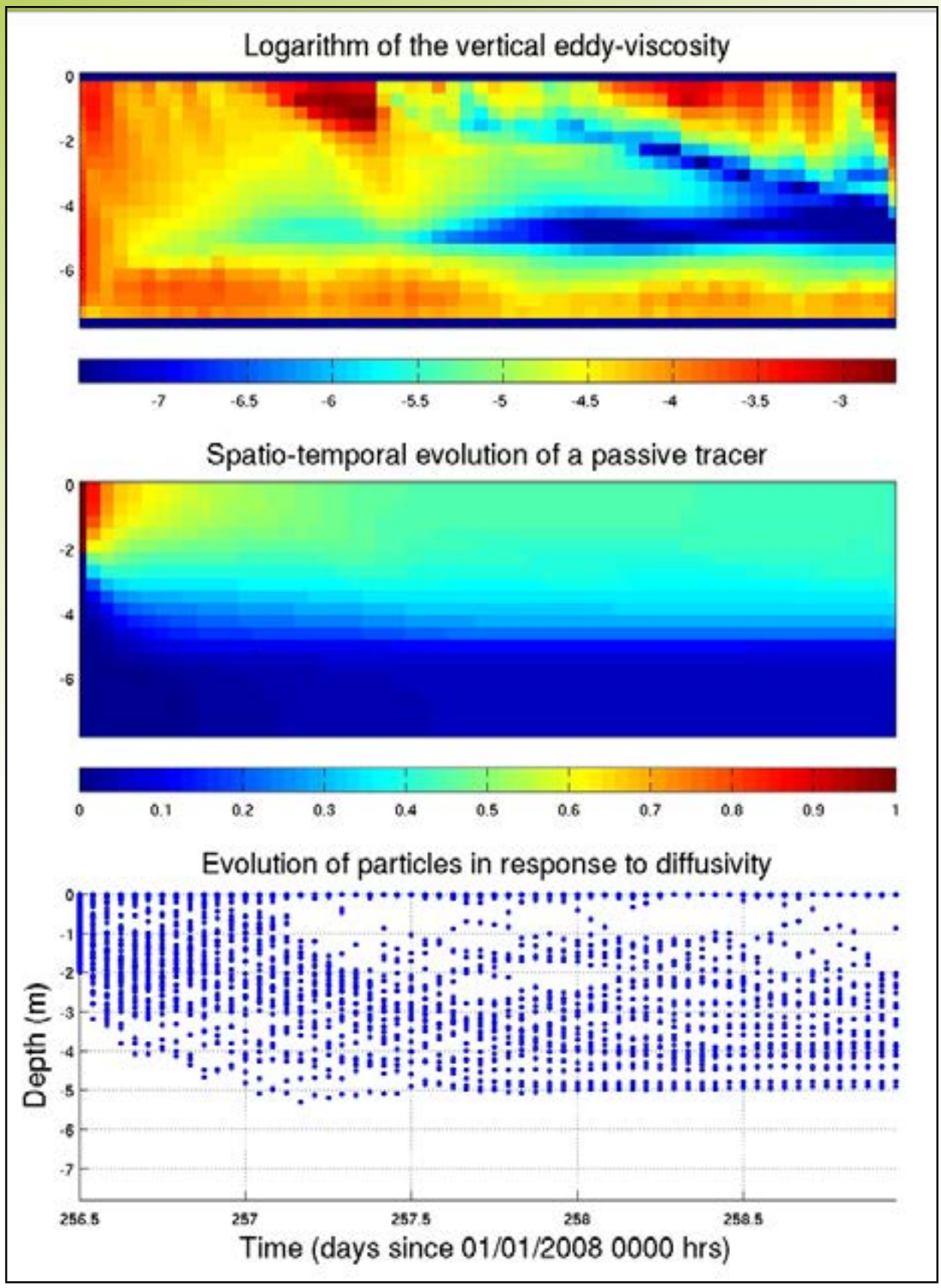

Figure E1 : Response of a passive tracer and a Lagrangian particle ensemble to average vertical eddy-viscosity (low, medium and high value) conditions.

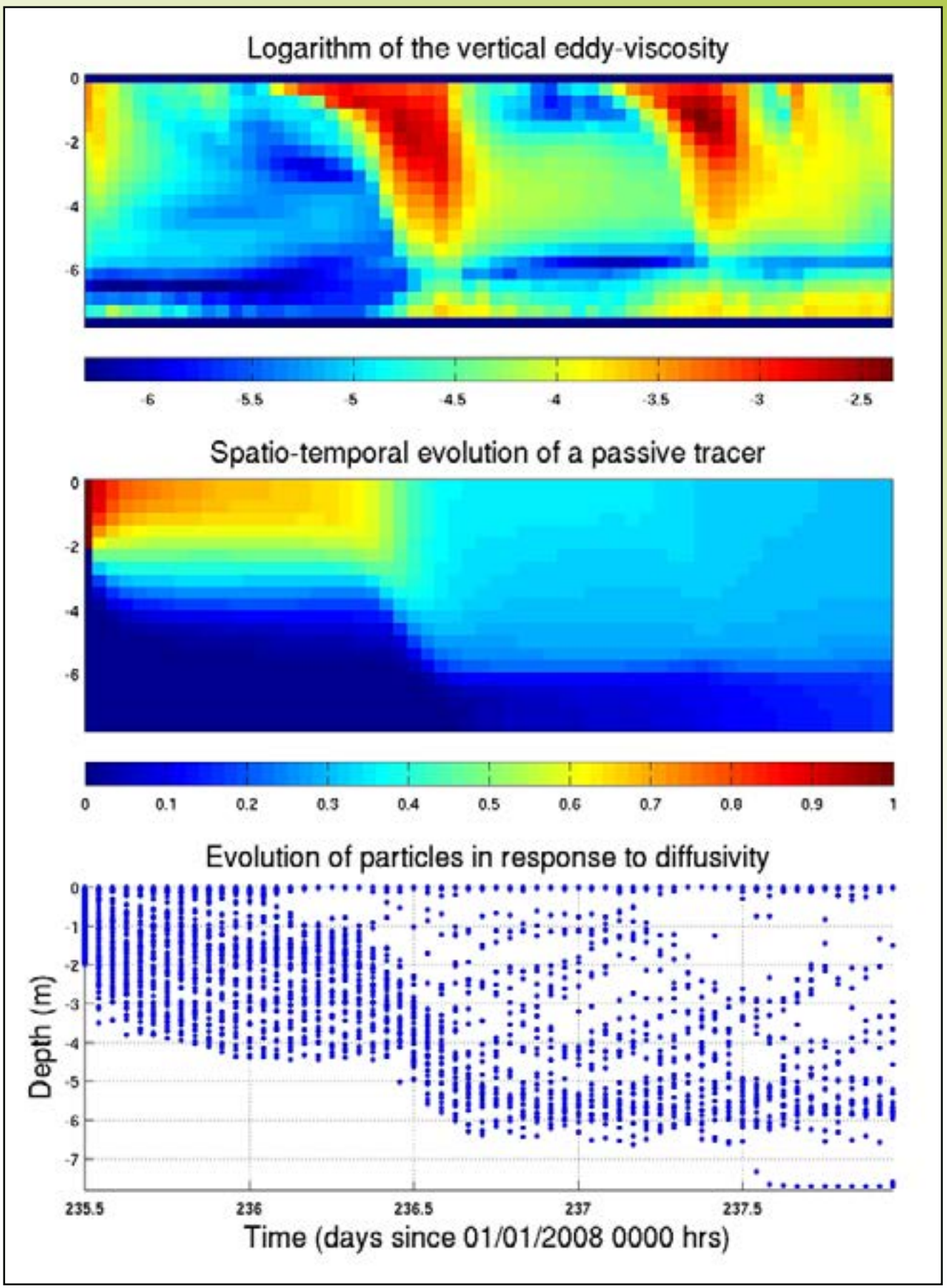

Figure E2 : Response of a passive tracer and a Lagrangian particle ensemble to low-moderate vertical eddy-viscosity conditions containing intermittent high values.

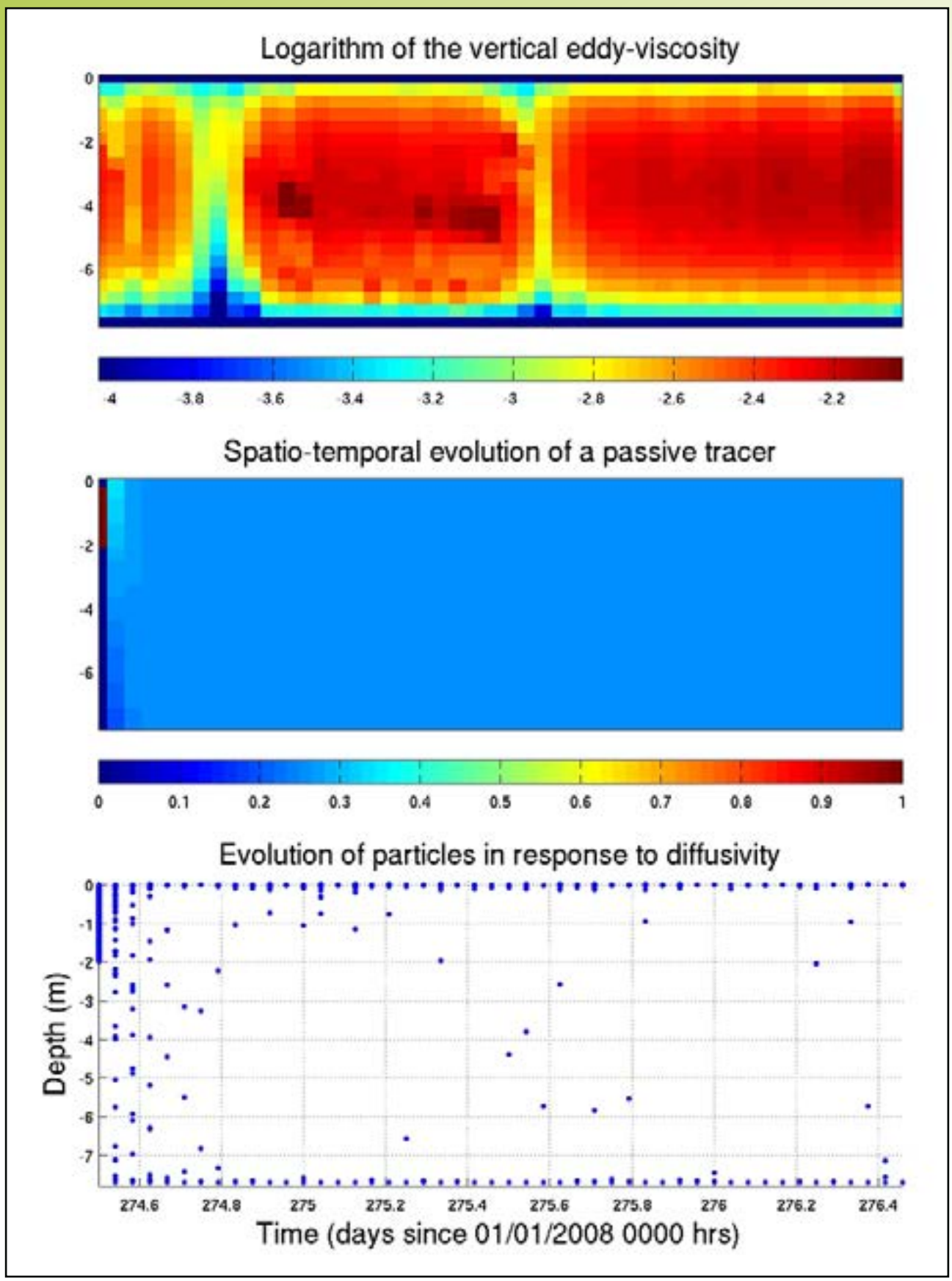

Figure E3 : Response of a passive tracer and a Lagrangian particle ensemble to consistently high vertical eddy-viscosity conditions.

A One-Dimensional Numerical Vertical Mixing Model with Application to Western Lake Erie

Lyon W. Lanerolle, Richard P. Stumpf, Timothy T. Wynne, and Richard C. Patchen
National Oceanic and Atmospheric Administration

A NOAA Technical Memorandum
NOS NCCOS 131
2011